

Review

# Recent Advances in Noble Metal Catalysts for Hydrogen Production from Ammonia Borane

Mengmeng Liu <sup>1,2</sup>, Liu Zhou <sup>1,2</sup>, Xianjin Luo <sup>3</sup>, Chao Wan <sup>1,2,3,4,\*</sup>  and Lixin Xu <sup>1,2,3,\*</sup>

<sup>1</sup> Hexian Chemical Industrial Development Institute, Engineering Research Institute, School of Chemistry and Chemical Engineering, Anhui University of Technology, Ma'anshan 243002, China; lmm0530@outlook.com (M.L.); iLiu97@hotmail.com (L.Z.)

<sup>2</sup> Ahut Chemical Science & Technology Co., Ltd., Ma'anshan 243002, China

<sup>3</sup> Anhui Haide Chemical Technology Co., Ltd., Ma'anshan 243002, China; AHUT.XJLuo@outlook.com

<sup>4</sup> College of Chemical and Biological Engineering, Zhejiang University, Hangzhou 310027, China

\* Correspondence: wanchao@ahut.edu.cn (C.W.); lxxu@ahut.edu.cn (L.X.); Tel.: +86-555-231-1807 (C.W.); +86-555-231-1521 (L.X.)

Received: 29 June 2020; Accepted: 13 July 2020; Published: 15 July 2020



**Abstract:** Interest in chemical hydrogen storage has increased, because the supply of fossil fuels are limited and the harmful effects of burning fossil fuels on the environment have become a focus of public concern. Hydrogen, as one of the energy carriers, is useful for the sustainable development. However, it is widely known that controlled storage and release of hydrogen are the biggest barriers in large-scale application of hydrogen energy. Ammonia borane ( $\text{NH}_3\text{BH}_3$ , AB) is deemed as one of the most promising hydrogen storage candidates on account of its high hydrogen to mass ratio and environmental benignity. Development of efficient catalysts to further improve the properties of chemical kinetics in the dehydrogenation of AB under appropriate conditions is of importance for the practical application of this system. In previous studies, a variety of noble metal catalysts and their supported metal catalysts (Pt, Pd, Au, Rh, etc.) have presented great properties in decomposing the chemical hydride to generate hydrogen, thus, promoting their application in dehydrogenation of AB is urgent. We analyzed the hydrolysis of AB from the mechanism of hydrogen release reaction to understand more deeply. Based on these characteristics, we aimed to summarize recent advances in the development of noble metal catalysts, which had excellent activity and stability for AB dehydrogenation, with prospect towards realization of efficient noble metal catalysts.

**Keywords:** ammonia borane; noble metal catalysts; chemical hydrogen; hydrogen production

## 1. Introduction

Energy is considered as a substantial material basis for survival and development of human society [1–3]. The rapid growth of world population and continuous improvement of living standard provokes excessive consumption of traditional fossil fuels, especially oil, coal and natural gas, as a matter of fact that in the future, these traditional resources will be inadequate to support the constantly progress of human civilization. Apart from the fact that fossil fuel resources are in short supply, many problems were exposed because of fossil fuel utilization [4,5], such as air pollution, water pollution and excessive carbon dioxide emissions leading to global warming. From this point of view, these problems have reached a serious point nowadays, thus, the exploitation of clean and renewable energy is receiving more attention.

Hydrogen, which is clean, effective and environmental benign nature [6–9], is regarded as an ideal alternative to fossil energy and the prospective secondary green energy in the 21st century. However, storage and transportation of large quantities of hydrogen are the difficult challenges [10–12],

which limit its advance and application. Hydrogen storage materials (mainly including chemical hydrides [13], adsorption hydrogen storage materials [14], metal hydrides [15], etc.) have been widely concerned and investigated [16–18]. In recent years, chemical hydride ( $\text{NH}_3\text{BH}_3$ ,  $\text{N}_2\text{H}_4$ , etc.), due to high hydrogen storage density, volume, have been proved to be a practical hydrogen source. Among them, ammonia borane is one of the most employed chemical hydrides, with providing safe and efficient alternative [19–21]. Ammonia borane ( $\text{NH}_3\text{BH}_3$ , AB), has a high capacity of hydrogen (19.6 wt%) [22,23], low molecular mass (30.7 g/mol) [24,25] and high solubility, which is a stable solid at normal atmospheric temperature, making it attractive candidate for hydrogen storage application. Moreover, AB with low condition of hydrogen production and various forms of decomposition has attracted intensive attention to explore.

The hydrolysis rate of AB is closely related to the selected catalysts [26]. The highly dispersed monometallic particles can improve the sites to achieve the effect of rapid hydrogen release. So far, more and more metal catalysts have been produced to accelerate the hydrolysis of AB. In this review, the progress of noble metal catalysts for the hydrolysis of AB was reviewed. At the same time, we introduced three kinds of decomposition methods of AB, including pyrolysis, alcoholysis and hydrolysis. Hydrolysis reaction is more widely used in the practical application for hydrogen production from AB. The development of new advance in single noble metal catalysts and composite catalysts of noble metals and non-precious metals were discussed, and the influence of using carbon, graphene, carbon nanotubes, silica, ceria and titanium supported catalysts on the hydrolysis of AB were explored. Finally, the inspiration for the future development of catalysts was given in this field.

## 2. The Processes of Hydrogen Production on $\text{NH}_3\text{BH}_3$ (AB)

### 2.1. The Methods of Producing Hydrogen from $\text{NH}_3\text{BH}_3$ (AB)

Through research and exploration, there are three main ways to release hydrogen from AB, pyrolysis, alcoholysis and hydrolysis, respectively [27–34].

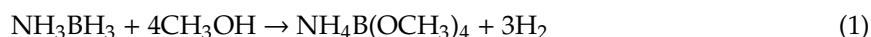
The pyrolysis process of solid phase thermal decomposition of AB [35–37] is shown in the following table (Table 1). Each reaction releases about one-third of the content, producing polyaminoborane, polyiminoborane, boron amide and other substances. When the temperature reaches 110 °C, AB begins to release its first equivalent of hydrogen, about 6.5 wt%. Intramolecular polymerization takes place at around 125 °C. When the temperature reaches 150 °C, the reaction releases a second amount of hydrogen. Finally, BN compounds are formed when the reaction temperature exceeds 500 °C [38]. In all, only the first and second processes are considered throughout the reaction, producing about 13% by weight of hydrogen. It is easy to produce borane, ammonia, bororazine and other harmful substances at high temperature, which is not conducive to environmental protection and practice application [39,40]. Contemporary, pyrolysis reaction as high temperature, high energy consumption and slow dehydrogenation power, is not suitable for mass manufacture.

**Table 1.** Ammonia borane decomposition of hydrogen.

Thermal Decomposition Step	Chemical Equation	Processes	Ref.
The first step (110 °C)	$\text{NH}_3\text{BH}_3 \rightarrow \text{NH}_2\text{BH}_2 + \text{H}_2$	The first yield of hydrogen	[35]
The second step (125 °C)	$n\text{NH}_2\text{BH}_2 \rightarrow (\text{NH}_2\text{BH}_2)_n$	Intramolecular polymerization	[36]
The third step (150 °C)	$(\text{NH}_2\text{BH}_2)_n \rightarrow (\text{NHBH})_n + n\text{H}$	The second yield of hydrogen	[37]
The remaining step (500 °C)	$(\text{NHBH})_n \rightarrow n\text{BN} + n\text{H}_2$	generation of excess hydrogen	[38]

Compared with pyrolysis, adding an appropriate catalyst, the alcoholysis of AB can release three equivalents of hydrogen at room temperature (Equation (1)) [41]. Chen et al. [42] prepared amorphous Co nanoparticles as catalyst for hydrogen liberation of AB alcoholysis, which displayed the intended hydrogen production performance. After ten tests of catalytic cycles, the turnover frequency (TOF) value of cobalt nanoparticles was still up to  $515 \text{ mol}_{\text{H}_2} \text{ mol}_{\text{metal}}^{-1} \text{ h}^{-1}$ . Yu et al. [43] synthesized CuNi

nanoparticles with a diameter of 16 nm by liquid phase method, which were successfully loaded onto graphene, and then obtained G-CuNi catalyst after being treated with tert-butylamine. It was surprising that the TOF value and activation energy of the catalyst reached up to  $49.1 \text{ mol}_{\text{H}_2} \text{ mol}_{\text{CuNi}}^{-1} \text{ min}^{-1}$  and  $24.4 \text{ KJ/mol}$ , respectively. Özhava et al. [44] reported that a stable Ni nanoparticles catalyst with polyvinylpyrrolidone (PVP) could be separated from the reaction solution by centrifugation, which had the advantages of simple preparation, high activity and high cost effectiveness. The TOF value of the catalyst utilized for the methanolysis of AB was  $12.1 \text{ min}^{-1}$ . The high production cost of alcoholysis even though adding catalysts can increase the rate of hydrogen releasing has drawn attention to solve the practice difficulties in promoting production.



AB hydrolysis is a process in which AB reacts with water in the presence of the suitable catalyst to release the hydrogen contained in the molecule [45]. The hydrolysis of AB to produce hydrogen can be carried out at room temperature, clean and pollution-free. Compared with the other two methods of hydrogen production, hydrolysis has obvious advantages, such as lower production cost, faster hydrogen liberation rate than alcoholysis and lower reaction temperature than pyrolysis [46]. This is an environmentally friendly and efficient hydrogen release method. AB reaction equation is as follows (Equation (2)). In the reaction process, the two hydrogen atoms in the hydrogen come from the AB molecule and the water molecule, and the hydrolysate is pollution-free. As a result, hydrogen production by hydrolysis of AB is considered to be an attractive approach to meet the low-cost and environmentally-friendly market needs.



## 2.2. The Hydrolysis Mechanism of $\text{NH}_3\text{BH}_3$ (AB)

The research on the hydrolysis mechanism of AB is mainly concluded by theoretical calculation and reasoning. Figure 1 showed the mechanism of hydrogen production by hydrolysis of AB. During the hydrolysis reaction, AB interacts with the catalyst surface to form a complex containing the H bond, and then in the attack of water, AB and  $\text{H}_2\text{O}$  each lose a hydrogen atom to form hydrogen [47]. Therefore, it can be found that the key step of catalytic water interpretation of hydrogen is that water molecules attack the M-H of the transition state. The properties of the metal catalyst M directly affect the formation of the transition state M-H and the speed of water interpretation of hydrogen. Thus, the catalysts are the key to whole hydrolysis reaction [48]. According to numerous literatures, the hydrolysis rate of AB is related to the amount of catalyst added, the amount of AB and the reaction temperature. Among them, temperature has the greatest influence on the hydrolysis rate, and the rate change can be obviously seen in the test of hydrogen release at different temperatures [49,50]. Generally speaking, the hydrolysis rate of AB has a zero-order relation or quasi-zero-order relation with the concentration of AB [51]. Highly dispersed metal particles can quite improve the hydrolysis rate, however the metal particles are easily agglomerated resulting in decreased catalytic activity. Mechanism studies show that AB interacts with metal particles and then dissociates the B-N bond in water to form  $\text{BO}_2^-$  and  $\text{H}_2$  [28].

The development of high performance, low cost and easy recovery catalysts are the key to realize the application of AB hydrolysate to obtain hydrogen. Xu [27] studied the performance of many metal catalyst systems on the generation of hydrogen by the hydrolysis of AB. The results presented that both noble metals and non-noble metals such as Pt, Ru, Pd, Rh, Cu, Co, Ni, etc. could be catalysts for the hydrolysis of AB [6]. Among them, noble metals were supposed to be potential candidate materials on account of their high chemical activity and stability, which were prominent in the hydrolysis reaction.

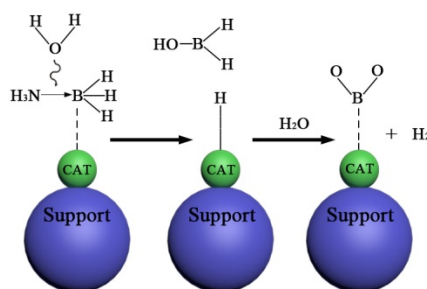


**Figure 1.** Mechanism of hydrogen production by ammonia borane (AB) hydrolysis.

Although non-noble metals have low costs, they exhibit low hydrogen generation rates in contrast to noble metals. What is more, their catalyst activities decline dramatically upon usage [52,53]. Hence, the utilization of noble metals is a consequence for high kinetics and stable hydrogen generation rate. Since there have been reports focused on catalytic hydrolysis of AB with noble metals [27], a number of studies have been conducted on monometallic and polymetallic catalysts [10]. Based on the above points, we mainly summarized the progress of high efficiency noble metal catalysts, composite catalysts and supported catalysts for AB dehydrogenation in the following papers.

### 3. The Development of Catalysts for $\text{NH}_3\text{BH}_3$ (AB) Dehydrogenation

In general, catalytic activity is evaluated based on the TOF value. TOF value is considered as the molecule that reacts per unit of active area in per unit time in the light of International Union of Pure and Applied Chemistry (IUPAC) [54]. In fact, the life of the catalyst is determined by the chemical, thermal and mechanical stability of the catalyst. However, as time goes on, the continuous accumulation of impurities or the loss of active particles on the surface of the catalyst will eventually lead to a decrease in the activity of the catalyst [55]. Therefore, it is desirable to find catalysts with excellent performance, which will remain stable and minimize deactivation after multiple reactions.

#### 3.1. Noble Metal Catalysts

Noble metal catalyst systems mainly refer to rare transition metal elements or multi-metal catalysts, as well as noble metal composite materials supported on other support materials. Pd [56], Pt [10,57–60], Ru [61–69] and Rh [70,71] are the main noble metal elements, which exhibit excellent performance in catalytic hydrolysis to produce hydrogen.

At the initial research, Xu's research team [27] found that noble metal showed high activity and stability in the AB hydrolysis catalyze process, which was due to the fact that the empty d-electron-orbitals contained in these elements were easy to absorb negatively charged protons and form intermediates to increase the reaction rate [72,73]. Among the many monometallic catalysts, the noble metals include Pd, Pt, Ru, Rh, showing high catalytic activity. On the other hands, Ru and Rh metals are often an alternative to the choice of precious metals, much slightly cheaper than that of noble Pt and Pd metals, at the same time, their catalytic effect can be comparable to noble metals.

Researchers are trying to improve the utilization rate and catalytic activity of noble metals to solve the problems of resource shortage and high price. Recently, investigators focused on preparing better and stable supported noble metal catalysts by selecting suitable carrier and adding additives [74–76]. On the basis of single metal, the dispersion of metal particles is strong, and the rate of hydrogen discharge increases significantly, by loading metal particles onto the carrier [77,78]. Poly(N-vinyl-2-pyrrolidone) (PVP) protected palladium rhodium nanoparticles with a size of 2.5 nm have been reported to be used as efficient catalysts [79], which provided the process of catalytic activity in the AB hydrolysis process and analyzed the generation of hydrogen. In the presence of PVP, the admixture of potassium tetrachloropropionate and rhodium chloride trihydrate was reduced by ethanol to Pd-Rh@PVP nanoparticles in ethanol water mixtures at reflux temperature. Among them, PVP was used as stabilizer and reducing agent. By comparing the catalytic activity of various

types (single metal Pd and Rh nanoparticles, their 1:1 physical mixture and 1:1 Pd-Rh bimetallic nanoparticles) in AB hydrolysis reaction, the formation of alloy type Pd-Rh@PVP nanoparticles has not been determined to be a physical mixture of single metal nanoparticles. Pd-Rh@PVP nanoparticles could be considered as a promising catalyst with the highest activity in realistic applications and could be used for proton exchange membrane fuel cell AB hydrolysis to produce hydrogen. Pd@PVP nanoparticles, Rh@PVP nanoparticle, 1:1 physical mixture Pd@PVP and Rh@PVP nanoparticles as well as Pd-Rh@PVP bimetallic nanoparticles respectively provided TOF values with growth trend: 182, 228, 430 and 1333. Figure 2 indicated that the hydrogen production presented linear relationship, starting immediately without induction period and continuing until complete hydrolysis of AB. It was worth noting that Pd-Rh@PVP nanoparticles with a concentration of 0.3 mM lead to the complete release of hydrogen in AB hydrolysis within 45 s, which was equivalent to an average TOF value of 1333 mol H<sub>2</sub> (mol cat)<sup>-1</sup> min<sup>-1</sup> at 25.0 °C. Compared with the physical mixture of Pd and Rh nanoparticles, Pd-Rh@PVP nanoparticles had higher catalytic performance, which was due to the effect of the synergy of Pd and Rh and the reduction of catalyst particle size. In addition, the Pd-Rh@PVP nanoparticle's catalyst maintained 78% of initial catalytic activity in AB hydrolysis, even after the fifth reaction.

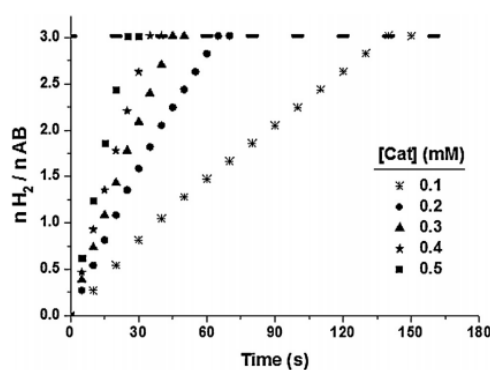


**Figure 2.** Plot of mol H<sub>2</sub>/mol AB versus time for the hydrolysis of 100 mM AB solutions in the presence of Pd-Rh@PVP nanoparticles in different catalyst concentrations (0.1, 0.2, 0.3, 0.4 and 0.5 mM) at 25.0 ± 0.1 °C; copyright (2014), Catalysis.

Because of its high hydrogen production activity in transition metal catalysts, platinum has attracted widespread attention [80,81], and been deeply studied by scholars. Kinetic studies and model calculations [57] show that Pt (111) facets are the main active surface. The particle size of about 1.8 nm is the optimal size of Pt. At the same time, the durability of the catalyst is closely related to the particle size of Pt [82–87]. The smaller the Pt particle size is, the lower its durability is, which may be related to the more obvious adsorption of B-containing species on the Pt surface and the easier the change of Pt particle size and shape. The results of this study paved the way for the rational design of highly active and durable platinum based catalysts for hydrogen production. Wang et al. [88] proposed a simple and gentle one-pot method to prepare porous PtPd bimetallic nanoparticles (NPs) with reverse structure under the adjustment of 1-hexadecyl-3-methylimidazolium chloride ([C<sub>16</sub>mim] Cl) in an aqueous solution. The composition and morphological concentration of PtPd NPs could be easily adjusted by changing the initial molar ratio of precursor and IL. In addition, by simply changing the content of glycine, they also found that it was possible to change the structure of porous PtPd NPs from Pt-on-Pt to Pt-on-Pd. Figure 3 revealed the possible growth mechanism of porous PtPd NPs in the presence of [C<sub>16</sub>mim] Cl. As shown in Figure 4, using various samples as catalysts, the hydrogen equivalent generated per mole of AB varies with the reaction time. It could be seen that AB maintained stability without hydrolysis in aqueous solution without any catalyst. Among all the catalysts used, porous Pt<sub>25</sub>Pd<sub>75</sub> NPs displayed the highest catalytic activity for AB dehydrogenation and hydrogenation. The reaction took only twelve minutes to complete and the hydrogen yield was as high as 97.3%. Porous Pt<sub>25</sub>Pd<sub>75</sub> NPs with a Pd-on-Pt structure could better combine with the B atom in AB to activate

the electronic B-H bond, making it easier to break the attack with H<sub>2</sub>O [89]. Due to its high specific surface area, porous layered structure (including mesopores and micropores) and possible electronic effects between Pt and Pd, porous Pt<sub>25</sub>Pd<sub>75</sub> NPs (Pd-on-Pt structure) had outstanding catalytic activity and the higher the stability of AB hydrolysis to produce hydrogen.

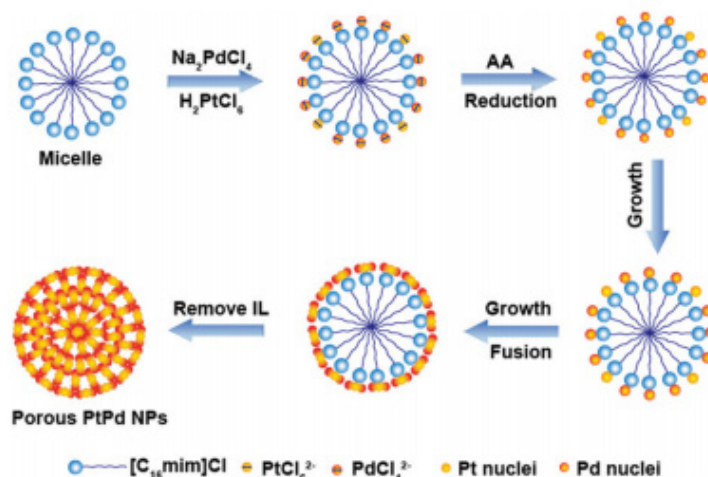


**Figure 3.** Illustration of the possible growth and assembly of the porous PtPd nanoparticles (NPs) in the presence of [C<sub>16</sub>mim] Cl; copyright (2020), the Royal Society of Chemistry.

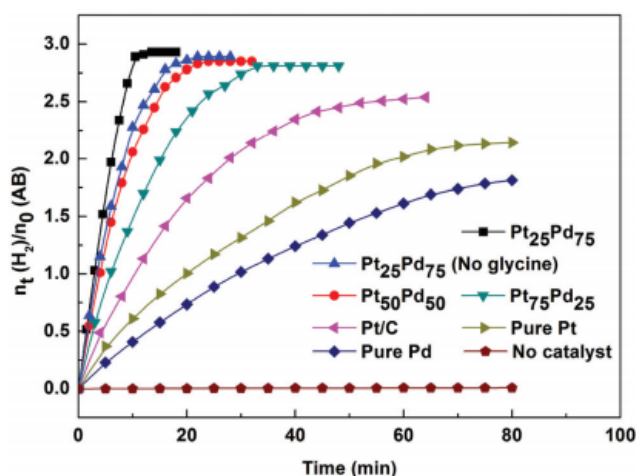


**Figure 4.** The curves of H<sub>2</sub> equivalents produced per mole of ammonia borane as a function of reaction time at 25 °C with various samples as catalysts; copyright (2020), the Royal Society of Chemistry.

Compared with platinum and palladium, ruthenium and rhodium are slightly cheaper, however their catalytic performance can be similar to those of them, which is ruthenium and rhodium being often used to replace platinum and palladium. In recent years, scholars have made extensive exploration on ruthenium and rhodium. Martina K, et al. [90] presented new Ru compounds having PNP amido chelate ligands, which could undergo reversible hydrogenation/dehydrogenation reaction both at the N functionality and the ethylene backbone. The reactivity of the ruthenium complexes was utilized for the homogeneous catalytic dehydrogenation of AB with excellent activities. Moreover, the catalysis of gold nanoparticles has attracted increasing attention because supported gold catalysts have been found having surprisingly high activity in oxidation. L.Wen et al. [91] successfully synthesized ultrafine Ru NPs deposited on MCM-41 via using a simple liquid impregnation reduction method. Furthermore, they determined the effect of different Ru content attached to MCM-41 on hydrolysis dehydrogenation of AB (0.52, 0.70, 0.90 and 1.12 wt%, respectively) (Figure 5). Among all results, 1.12 wt% Ru/MCM-41 presented the highest catalytic activity, with TOF value of 288 min<sup>-1</sup>. In summary, Ru/MCM-41

appeared excellent catalytic activity toward hydrolysis of AB owing to the unique structure of MCM-41 with ordered hexagonal pores and the strong synergistic effect.

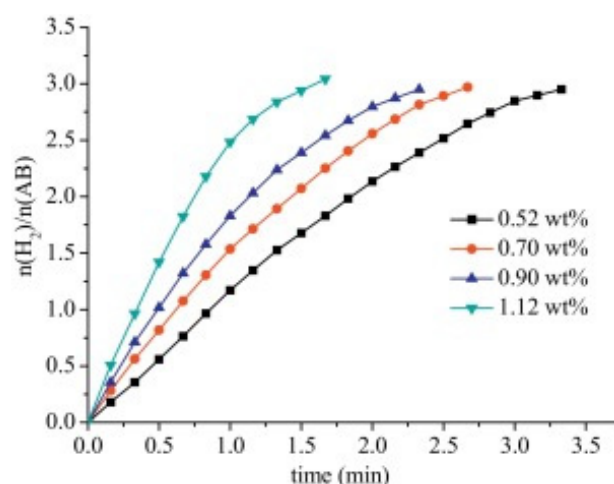


**Figure 5.** Hydrogen generation from aqueous AB in the presence of Ru/MCM-41 catalysts at room temperature. Ru/AB (molar ratio) = 0.0026, 0.0044, 0.0045 and 0.0055 at Ru loadings of 0.52, 0.70, 0.90 and 1.12 wt%; copyright (2015), Chinese Chemical Letters.

In the literature on catalytic hydrolysis of AB with support Ru catalysts, their catalytic activities are related to many factors, including particle diameter and location distribution, as well as preparation method and selection of load carrier [92,93]. Late transition metal nanoparticles (NPs) are more prone to aggregate in solution [94,95]. Although it can be alleviated by adding or supporting substances, the effective area of NPs will be reduced by retention matching, which will affect the catalytic chemical reaction [96]. Abo-Hamed E K. et al. [97] reported a monodisperse metastable ruthenium nanoparticle (Ru NPs), which could easily solve these problems. Their report represented the case in which Ru NPs remained stable without protective ligands or carriers while simultaneously exhibited high catalytic activity. Metastable Ru NPs have been proved to be a promising catalytic active material for production of hydrogen via hydrolysis of AB at room temperature. Shen et al. [76] have produced a one-step in situ route for synthesis Rh nanoparticles supported on graphene by using methylamine borane (MeAB) (Figure 6a,b). Compared with conventional carriers, prepared Rh/NPs supported on graphene exhibited better catalytic activity on hydrolysis of AB, with high TOF values of  $325 \text{ min}^{-1}$  and low activation energy ( $E_a$ ) values of  $16.4 \text{ KJ mol}^{-1}$ . As clearly shown from transmission electron microscope (TEM) image of Rh/graphene NPs, there were no significant changes in morphology of Rh/NPs on graphene, and no noticeable aggregation of Rh/NPs after the fifth run durability (Figure 6c,d).

### 3.2. Noble Metal and Non-Precious Metal Composite Catalysts

Noble metal catalysts exhibit high catalytic capability, but the high cost and low utilization of precious metals have greatly limited their application in commercial production [98]. Whereas non-precious metals are favored by researchers on account of the abundant resources on earth and low price, even if their catalytic property are not as good as noble metals. To address effectiveness of catalysts [99], it is better to add non-precious metals to the catalysts without significantly reducing the catalytic activity to manufacture noble metal and non-precious metal composite catalysts. Although the hydrolyzing rate of AB can be improved obviously by using non-noble metal materials or composites as catalysts, the catalytic performance of non-precious metal catalysts has yet to be advanced compared with noble metals. Now, how to improve the catalytic activity of cheap non-precious metals has become a popular topic. Pure noble metals and non-precious metals have not been able to meet the requirements of market, thus, the combination of noble metals and non-precious metals or mutual

fusion for solution provides ideas to solve this matter. Then binary or multivariate catalysts gradually emerged [100,101], which not only reduce the material cost, but also enhance catalyst activity.

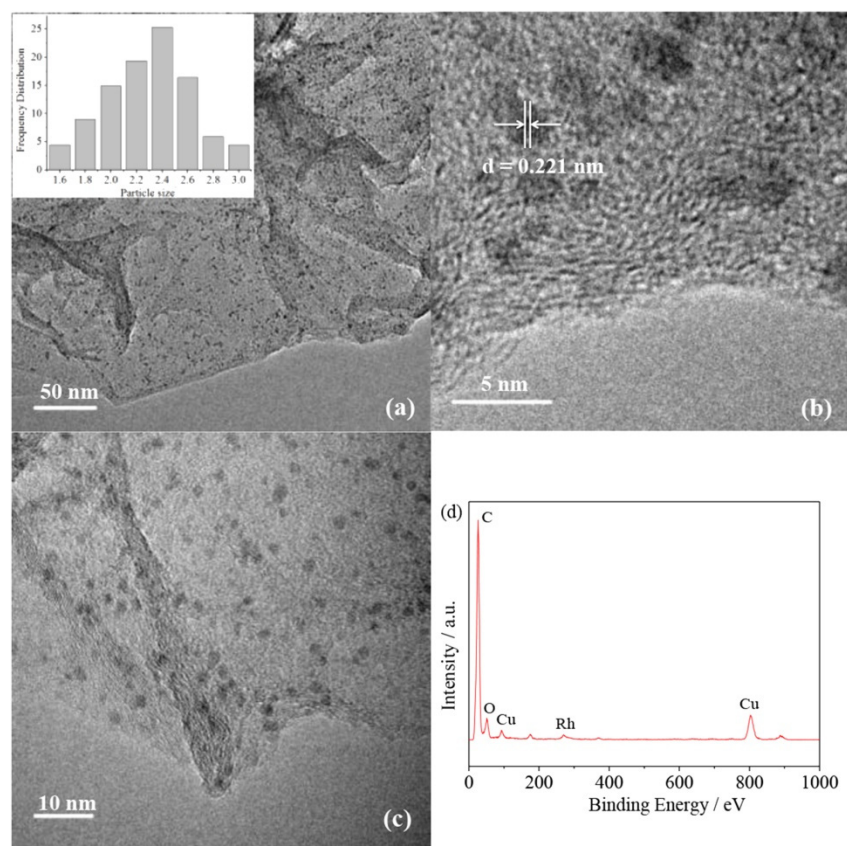


**Figure 6.** (a) and (b) TEM and HRTEM images of the Rh/graphene NPs; (c) TEM mages of the Rh/graphene NPs after five cycles; (d) EDS spectrum of Rh/graphene NPs; and (a) inset: particle size distribution of Rh/graphene NPs; copyright (2014), Hydrogen Energy.

Manna et al. [56] used cobalt-ferrite coated by polydopamine (PDA) as the carrier, which was the coating layer formed by the long-term mixing of dopamine hydrochloride and cobalt ferrite, and then loaded palladium particles onto the carrier to synthesize Pd/PDA-CoFe<sub>2</sub>O<sub>4</sub>. The results displayed that Pd/PDA-CoFe<sub>2</sub>O<sub>4</sub> with Pd loading of 1.08 wt% was a highly active and reusable catalyst. Moreover, it was worth mentioning that Pd still maintained its initial catalytic activity after ten times of catalysis. Zhang J et al. [102] fabricated Pd-Cu nanocrystals by a facile and flexible protocol, with diverse morphological features to enhance catalytic and durability. As a result that elements Pd (2.20) and Cu (1.91) were significantly different in the electronegativity, it was easier to generate electrons from one element to another after forming the alloy, resulting in the electron coupling effect. Through the characterization technology, X-ray photoelectron spectroscopy (XPS) analysis results are confirmed in Figure 6. As could be seen from Figure 7, there was indeed an electric coupling or synergistic effect in Pd-Cu alloy, which was conducive to the adsorption of H to form metal-H species, thereby promoting the catalytic effect of AB hydrolysis. In theory, it was the accumulation of electron clouds around the nucleus of Pd that promoted the adsorption of H and facilitated the formation of metal-H species to accelerate the dehydrogenation of AB [103]. Furthermore, the catalytic activity of AB was investigated in detail using Pd-Cu alloy nanocrystals as catalysts. The hydrogen equivalent produced from AB hydrolysis by six different Pd-Cu alloy nanocrystals (Pd-Cu NAs-1, Pd-Cu NAs-2, Pd-Cu NAs-3, Pd-Cu NAs-4, Pd-Cu NAs-5, Pd-Cu NAs-6) prepared them and metal nanocrystals of two elements (Pd-NPs, Cu-NPs) were shown in Figure 8. For all the catalysts investigated, the catalytic capacity of Pd-NPs was the strongest, while that of Cu-NPs was the weakest. In bimetallic alloy nanocrystals,

Pd-Cu NAs-1 held the highest catalytic ability. For bimetal Pd-Cu alloy nanocrystal catalytic capacity follows the following order: Pd-Cu NAs-1 > Pd-Cu NAs-5 > Pd-Cu NAs-2 > Pd-Cu NAs-3 > Pd-Cu NAs-4 > Pd-Cu NAs-5. By this treating, experimental data confirmed, actually, the fact that catalytic performance of bimetallic catalysts was superior to that of their single metal elements, which has been recorded in other literature on other alloy catalysts [104,105].

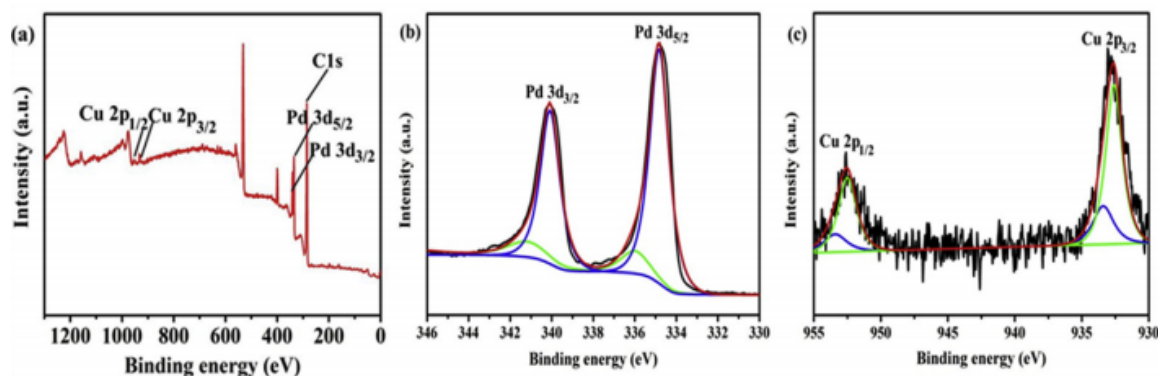


**Figure 7.** XPS spectra for the Pd-Cu NAs-1 sample. (a) Survey scan; (b) Pd 3d; (c) Cu 2p; copyright (2019), Hydrogen Energy.

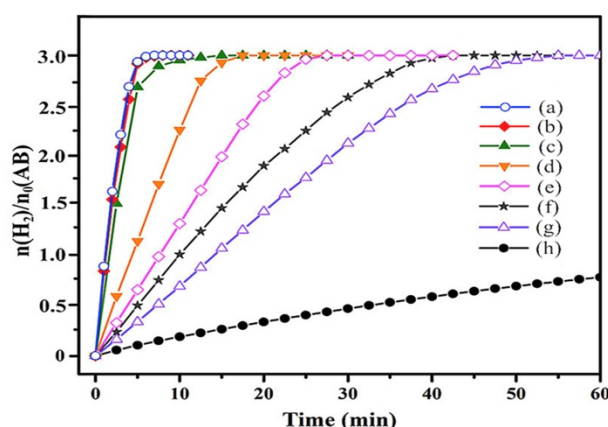


**Figure 8.** H<sub>2</sub> equivalents generated from AB hydrolysis catalyzed by the different Pd-Cu alloy nanoparticles at 298 K. (a) Pd-NPs; (b) Pd-Cu NAs-1; (c) Pd-Cu NAs-5; (d) Pd-Cu NAs-2; (e) Pd-Cu NAs-3; (f) Pd-Cu NAs-4; (g) Pd-Cu NAs-6; (h) Cu-NPs; copyright (2019), Hydrogen Energy.

Compared to monometallic catalysts, much better selectivity and catalytic activity have been demonstrated for bimetallic catalysts [106–110]. The bimetallic catalysts formed by Pt and non-precious metal have been proved to be superior to other catalysts. Yang's group [111] reported that Pt<sub>x</sub>Ni<sub>1-x</sub> ( $x = 0, 0.35, 0.44, 0.65, 0.75$  and  $0.93$ ) nanoparticles were used as catalyst for hydrogen generation from hydrolysis of AB. They studied the catalytic activity of Pt<sub>x</sub>Ni<sub>1-x</sub> ( $x = 0, 0.35, 0.44, 0.65, 0.75$  and  $0.93$ ) the hydrolysis and dehydrogenation of AB solution. The results exhibited that the particle size of Pt<sub>x</sub>Ni<sub>1-x</sub> nanoparticles were about 2–4 nm, and the contents of Pt atom in the catalyst were 35%, 44%, 65%, 75% and 93%, respectively. It was found that catalytic activity of AB hydrolysis was related to the composition of Pt<sub>x</sub>Ni<sub>1-x</sub> catalyst and Pt<sub>0.65</sub>Ni<sub>0.35</sub> nanoparticles have the highest catalytic activity. The activity of the synthesized Pt<sub>x</sub>Ni<sub>1-x</sub> catalyst was better than that of pure Pt or Ni catalyst. The TOF value and the E<sub>a</sub> of the reaction were 4784.7 mL min<sup>-1</sup> g<sup>-1</sup> and 39.0 KJ/mol. Gao M et al. [112] prepared monodisperse PtCu alloy NPs and explored the action of their catalysts for hydrolysis AB under mild condition. Among different composition PtCu NPs, the Cu<sub>50</sub>Pt<sub>50</sub> NPs as optimum catalyst demonstrated the highest catalytic performance with an initial TOF of 102.5. These experimental results exhibited that the validity of partly replacing Pt by a first-row transition metal on designing superior

property heterogeneous nanocatalysts for AB hydrolytic. Chen et al. [113] designed Pt-WO<sub>3</sub> double active site catalyst to boost the catalytic hydrolysis of AB. Figure 9 showed the hydrolysis mechanism of AB on Pt double activity. Pt-WO<sub>3</sub>/CNT could significantly improve hydrogen production activity and durability, which was attributed to the double active center of Pt-WO<sub>3</sub> and the sacrifice site of WO<sub>3</sub>.

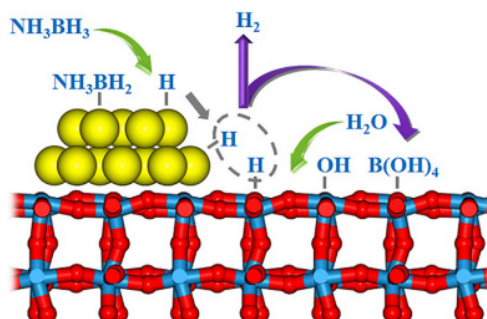


**Figure 9.** A Proposed Mechanism for Ammonia Borane Hydrolysis over Pt-WO<sub>3</sub> Dual Metal Sites; copyright (2020), Elsevier.

Transition metal nanoparticles are widely applied in the hydrolysis AB [114,115]. However, in the catalytic process, metal particles can aggregate to form clumps, which will lead to the inactivation of catalyst, the existence of instability and low efficiency [116]. In order to avoid the influence of low repetition rate, the nanoparticle's catalyst was prepared by using magnetic powder as the catalyst active metal carrier so as to become the magnetic separable catalyst in the liquid phase reaction, which can enhance the rate of catalysts utilization [117–119]. Hence, Akbayrak S et al. [120] reported three metal(0) nanoparticle catalysts formed by loading ruthenium(III), rhodium(III) and palladium(II) onto magnetic carriers of iron coated with carbon(C-Fe) at room temperature as transition metal nanoparticles for hydrolysis of AB, M<sup>0</sup>/C-Fe NP(M=Ru, Rh and Pd). Using the XPS, energy dispersive X-ray detector (EDX), TEM techniques, the results of tests showed that Rh<sup>0</sup>/C-Fe (0.45% wt. Rh), Ru<sup>0</sup>/C-Fe (1.59% wt. Ru) and Pd<sup>0</sup>/C-Fe (2.0% wt. Pd) nanoparticles gave TOF of 83, 93 and 29 min<sup>-1</sup>, respectively. In the repeatability tests, M<sup>0</sup>/C-Fe remained premier activity even after hydrolysis reactions, as shown in Figure 10. In this review, M<sup>0</sup>/C-Fe nanoparticles revealed outstanding reusability and activity.

Zhou Q et al. [121] prepared nanoporous ruthenium (NP-Ru), which was consisted of an interconnected nanoscaled ligament by one-step mild etching of RuAl alloy. NP-Ru showed high catalytic activity at room temperature and had a long life to hydrolyze AB. In addition, it was found that even after five runs, NP-Ru still had excellent reusability and recyclability, and its original catalytic activity was 67%. Wei Z et al. [122] proposed a simple method for preparing CoRu nanoalloy catalysts (CoRu@N-C) by encapsulating the alloy material into carbon layer. With this strategy, CoRu nanoalloy catalysts could effectively prevent the alloy from accumulating in the corrosive medium and facilitate the catalytic reaction on the surface. Moreover, CoRu@N-C exhibited excellent sustainability and high catalytic performance for hydrolysis of AB.

It has been dedicated to the exploration of bimetallic catalysts for AB catalytic dehydrogenation [123–127]. A variety of bimetallic catalysts have better catalytic performance than single metal catalysts, however, the catalytic efficiency of AB as a hydrogen storage candidate is still far from meeting the needs of practical applications. Au-containing hybrid materials have received great attention from scholars due to their unique synergy. For example, the contact between Au NPs and metal oxides improved the high catalytic activity of inert gold [128–131]. Introducing Au clusters into vulnerable parts or subsurface of Pt and Pt-TM nanocatalysts greatly improved the electrochemical stability of the catalyst [132–135]. By introducing Au into the Pt-TM nanocatalysts, it was reasonable to speculate that it has superior catalytic performance for AB catalytic dehydrogenation. Zhai et al. [136] succeeded in obtaining a PtAuCo trimetallic nano-alloy with a single-phase structure through a sequential digestion and reduction strategy. Figure 11 illustrated the formation mechanism

of single-phase PtAuCo trimetallic alloy catalyst. In order to evaluate the performance of the catalyst for AB hydrolysis, they tested the activity of the prepared PtAuCo nanocatalyst with single metals (Pt, Au, Co) and bimetals ( $\text{Pt}_{85}\text{Au}_{15}$ ,  $\text{Pt}_{86}\text{Co}_{14}$ , Au@Co) based on 298 K. As shown in Figure 12a,b, the activity of bimetallic nanocatalysts was better than that of single metal nanoparticles. Moreover, the reinforcement of the nanoalloy structure was superior to that of the core-shell structure.  $\text{Pt}_{85}\text{Au}_{15}$  and  $\text{Pt}_{84}\text{Co}_{16}$  have almost the same metal ratio, nevertheless, the TOF value of the former ( $\sim 137 \text{ mol H}_2 \text{ min}^{-1} (\text{mol metal})^{-1}$ ) was much higher than the latter ( $\sim 66 \text{ mol H}_2 \text{ min}^{-1} (\text{mol metal})^{-1}$ ), indicating that the activity enhancement efficiency of Au was very high. Figure 12c,d showed that when about 10% of Pt in  $\text{Pt}_{84}\text{Co}_{16}$  was replaced by Au to form a  $\text{Pt}_{76}\text{Au}_{12}\text{Co}_{12}$  trimetallic nanoalloy, the hydrogen evolution reaction of AB was completed within 36s and the TOF value was increased to  $450 \text{ mol H}_2 \text{ min}^{-1} (\text{mol metal})^{-1}$ . In all synthetic samples,  $\text{Pt}_{76}\text{Au}_{12}\text{Co}_{12}$  showed the best catalytic performance for the catalytic hydrolysis of AB. In addition, they used XPS technology to systematically measure the trimetallic catalysts with different compositions and corresponding monometallic and bimetallic counterparts, in order to explore the underlying mechanism. The results exhibited that the main reason for the excellent catalytic performance of  $\text{Pt}_{76}\text{Au}_{12}\text{Co}_{12}$  catalyst was the modified electronic interaction and enhanced charge transfer ability.

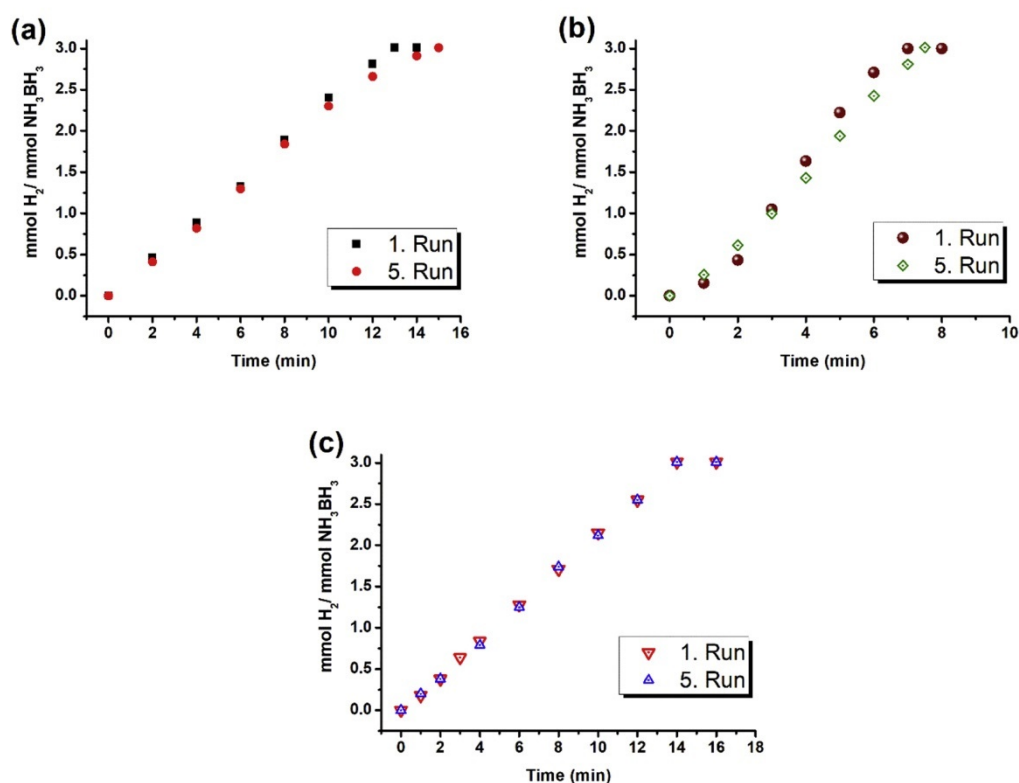


**Figure 10.** Hydrogen evolution plots (mmol H<sub>2</sub>/mmol AB vs. time) for the first and fifth run of hydrolysis starting with (a) Rh<sup>0</sup>/C-Fe NPs; (b) Ru<sup>0</sup>/C-Fe NPs; (c) Pd<sup>0</sup>/C-Fe NPs at 25.0 °C; copyright (2020), Hydrogen Energy.

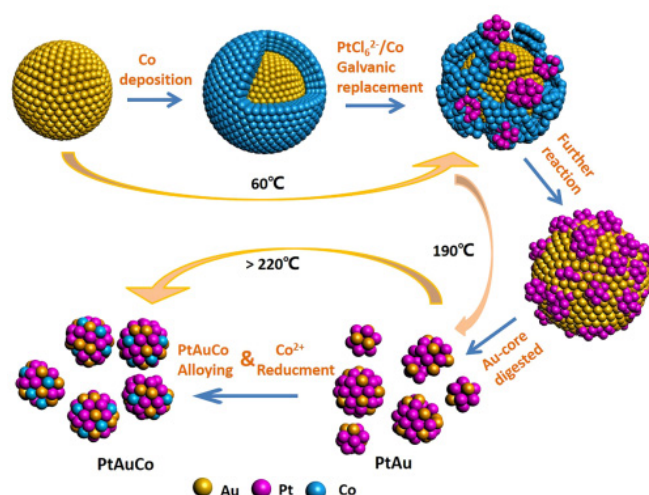


**Figure 11.** Fabrication strategy of the PtAuCo trimetallic alloys; copyright (2020), American Chemical Society.

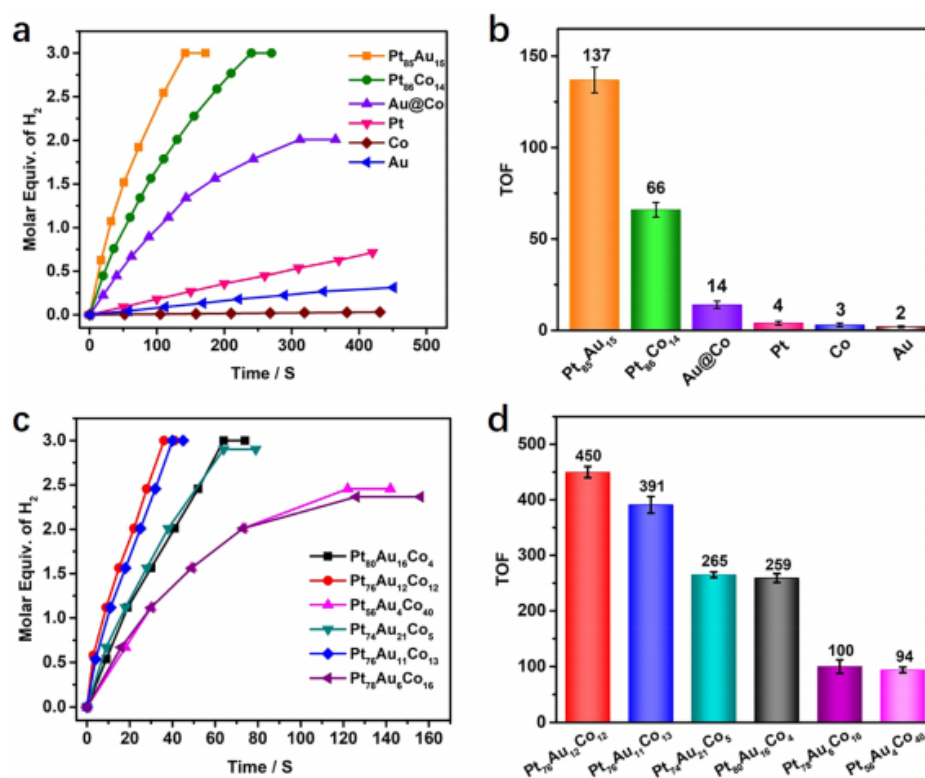


**Figure 12.** (a,c) Plots of time vs.  $H_2$  generation and (b,d) the corresponding TOF value of the AB hydrolysis reaction at 298 K catalyzed by (a,b) the monometallic (Pt, Au, Co) and bimetallic ( $Pt_{55}Au_{15}$ ,  $Pt_{86}Co_{14}$ , Au@Co) catalysts and (c,d) the trimetallic catalysts of different composition; copyright (2020), American Chemical Society.

In summary, according to numerous literatures, the hydrolysis of noble metals for the dehydrogenation of AB revealed excellent activity. However, the defects of noble metals have restricted their widespread adoption. It is worth noting that the combination of noble metals and non-precious metals to form a supported catalyst can not only settle the resource shortage of precious metals, but also reduce the material cost [137–139]. Furthermore, the supported catalysts greatly improve the catalytic capacity of AB due to adjust the electronic structure and surface geometry to

adjust the catalytic performance [140–142]. Therefore, the supported catalysts of AB catalytic hydrolysis are the focus of research and development in the future.

### 3.3. Catalytic Activities of Supported Metal Catalysts in $\text{NH}_3\text{BH}_3(\text{AB})$ Hydrolysis

On the basis of the metal catalyst, by loading the metal particles on the support, the dispersion of the metal particles is improved, and the hydrogen release rate is significantly increased [143]. Due to its porous structure, the carrier materials increase the specific surface area between the metal nanoparticles and delay the formation of impurities on the nanoparticles, ultimately preventing the agglomeration of the nanoparticles [144]. The supports commonly used are graphene, carbon, carbon nanotubes (CNT), silicon, cerium, titanium [145–150].

#### 3.3.1. Graphene Material Supported Metal Catalysts

Graphene is a single-atom honeycomb lattice-like carbon material with a surface area of  $2600 \text{ m}^2 \text{ g}^{-1}$  [151]. In addition, it is suitable for supporting materials based on the characteristics of high mechanical strength, excellent electrical conductivity [152], outstanding thermal stability and chemical stability [153]. Through burdening metal nanoparticles on graphene, it can prevent its polymerization and improve its catalytic activity. In this way, in addition to increasing the superficial area of the catalysts, the accelerated charge transfer at the graphene metal interface is also conducive to promote catalytic activity [154]. Nowadays, there were a lot of literatures about the application of graphene loaded metal catalysts in AB hydrolysis. Chemical derived graphene (CDG) was synthesized by reduction of graphene oxide with hydrazine hydrate and used as the carrier of palladium nanoparticles (Pd NPs) [145]. By advanced analytical technology, Pd NPs keeping particle size dispersion and stability loaded onto CDG was used as catalyst for AB dehydrogenation and hydrolysis. Using CDG-Pd as a catalyst, the AB dehydrogenation and hydrolysis hydrogen production processes were tested, and it was found that CDG-Pd had high activity in both dehydrogenation and hydrolysis reactions. Figure 13 showed the graph of the molar  $\text{H}_2/\text{mol AB}$  ratio with time during the catalytic dehydrogenation and hydrolysis of 2.0 mmol AB solution in taking advantage of CDG-Pd catalyst (2.1% wt Pd) at  $25^\circ \text{C}$ . Under existence of CDG-Pd catalyst, the dehydrogenation of AB produced one equivalent of hydrogen, while the hydrolysis of AB produced three equivalent of hydrogen. In the presence of CDG-Pd catalyst, the calculated values of AB for the initial TOF of dehydrogenation and hydrolysis were  $170 \text{ h}^{-1}$  and  $933 \text{ h}^{-1}$ , respectively (Figure 13). These values were comparable to the AB dehydrogenation and hydrolysis catalyst system. In addition to its high activity and stability, CDG-Pd was also found to be a reusable catalyst in dehydrogenation and hydrolysis. After the 5th and 10th runs, the hydrolysis of AB remained its initial activity of 85% and 95%, respectively, which made CDG-Pd have broad application prospects in noble metals to be used as a catalyst to develop an available portable hydrogen production system employing AB as a solid hydrogen storage and release material.

Ked et al. [155] reported a new type of high-efficiency catalyst for the hydrolysis of AB to produce hydrogen by embedding Pt-Co nanoparticles in nanoporous graphene sheets. In order to expound the formation mechanism of Pt-Co@PG catalyst, Figure 14 showed the steps of preparing Pt-Co NP aggregated on nanoporous graphene (PG) sheets, which included two important steps: preparing nanoporous graphene sheet by carbothermal metal oxide etching method, and then uniformly embedding Pt-Co nanoparticles into plane and holes defects. They studied the catalytic properties of Pt-Co bimetallic NPs supported in nanoporous graphene (Pt-Co@PG) and the catalytic dehydrogenation performance in AB aqueous solution. It was critical important to study the preparation of NP embedded in porous graphene and the synergistic effect between them. They used prepared nanoporous graphene loaded pure Pt NP, pure Co NP and Pt-Co NP to catalyze the hydrolysis of AB (1.5 mmol, 6 mL), respectively. Figure 15a displayed the amount of hydrogen produced during the process of hydrolytic dehydrogenation using the prepared  $\text{Pt}_x\text{Co}_{1-x}$ @PG NP. Obviously, pure PG had no catalytic activity for AB hydrolysis, and the hydrogen release rate of Pt-Co@PG NPs was much higher than that of pure Co@PG NPs, which indicated that Pt was a more effective element for AB hydrolysis. The catalytic

mechanism of Pt-Co bimetallic NPs could be attributed to the synergistic effect of Co and Pt, which was triggered by the charge interaction between Pt Co NPs and PG carrier and the reduced particle size (providing rich active sites) [156]. Therefore, in the catalysis of Pt Co bimetallic NPs heterogeneous reaction, the catalyst with the best ratio of Pt and Co showed the highest catalytic activity. Pt<sub>0.1</sub>Co<sub>0.9</sub>@PG achieved the best performance, which had obvious high catalytic activity to release hydrogen in three minutes hydrolysis AB, with TOF value as high as 461.17 mol<sub>H<sub>2</sub></sub> min<sup>-1</sup> mol<sub>Pt</sub><sup>-1</sup>. As shown in Figure 15b, compared with the bare Pt<sub>0.1</sub>Co<sub>0.9</sub> catalyst and the reduced graphene oxide supported Pt<sub>0.1</sub>Co<sub>0.9</sub> catalyst, supporting function of nanoporous graphene had been clearly demonstrated. Recent studies showed that the enhanced catalytic activity of graphene supported metal nanoparticles was attributed to the interface interaction between metal nanoparticles and graphene materials [33]. The nanoporous graphene sheet provided more edges related to the presence of pores and more anchoring agents to stabilize Pt-Co nanoparticles with uniform dimensions. The simple synthesis, excellent catalytic performance revealed that the Pt-Co@PG nano hybrid material was a promising candidate material for the development of highly efficient and portable AB hydrogen production system.

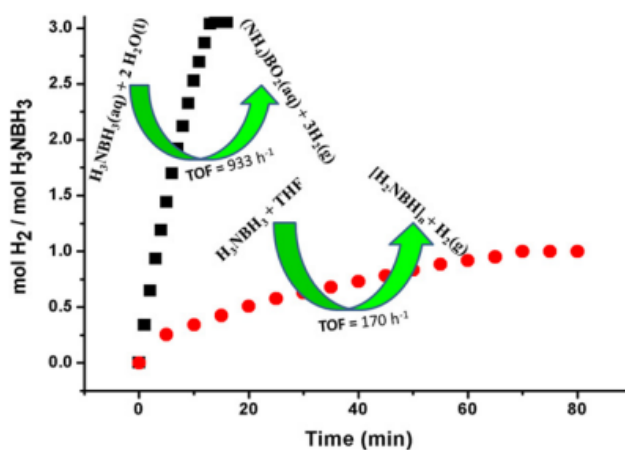


**Figure 13.** The mol H<sub>2</sub>/mol H<sub>3</sub>NBH<sub>3</sub> versus time plots for the dehydrogenation and hydrolysis of AB catalyzed by CDG Pd (2.1% wt Pd); copyright (2012), Elsevier.

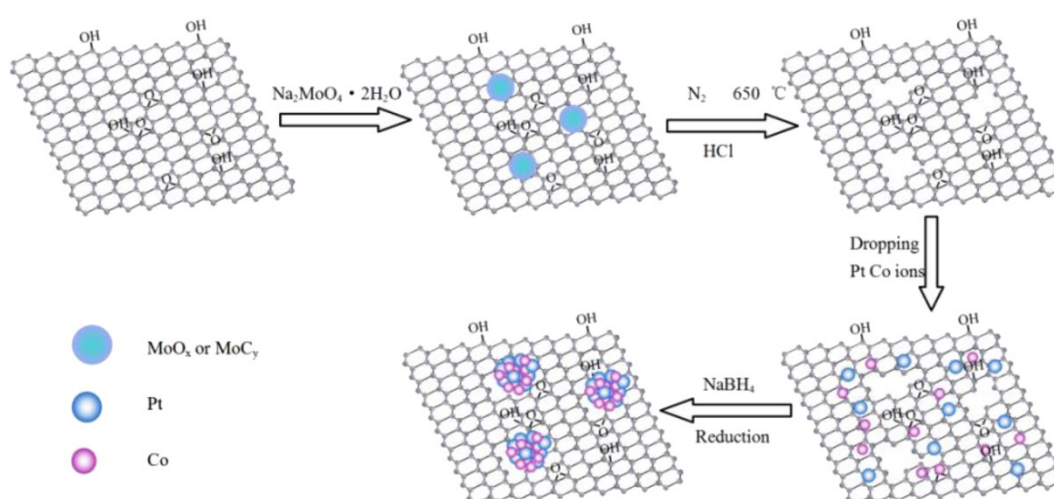


**Figure 14.** Mechanism of Pt-Co@PG catalyst preparation; copyright (2017), Elsevier.

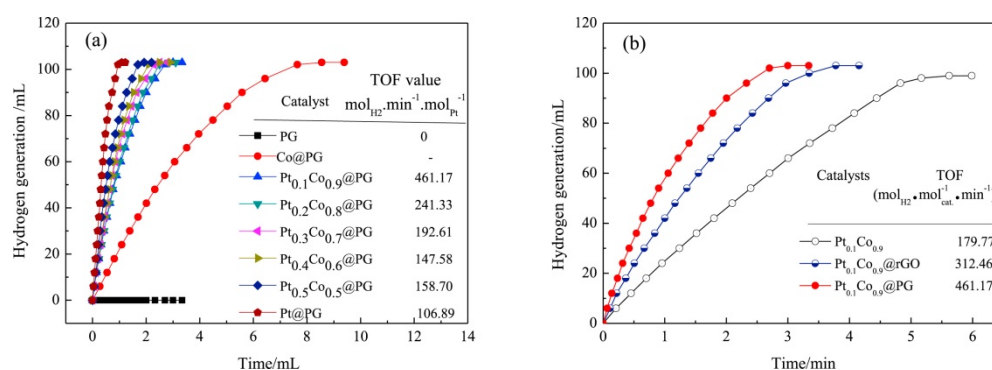


**Figure 15.** (a) Hydrolysis of aqueous  $\text{NH}_3\text{BH}_3$  solution under ambient atmosphere catalyzed by pure Pt@PG NPs, pure Co@PG NPs and Pt-Co@PG NPs with different ratios; (b) hydrolysis of aqueous  $\text{NH}_3\text{BH}_3$  solution catalyzed by Pt<sub>0.1</sub>Co<sub>0.9</sub> NPs, Pt<sub>0.1</sub>Co<sub>0.9</sub>@GO NPs and Pt<sub>0.1</sub>Co<sub>0.9</sub>@PG; copyright (2017), Elsevier.

### 3.3.2. Carbon Material Supported Metal Catalysts

Due to these performance that the modified surface chemistry [60] (such as defects and oxygen groups), texture characteristics (such as aperture), outstanding thermal conductivity and resistance to acid and alkaline environment [157], scholars are keen on exploiting carbon-based materials as catalyst carriers. Carbon is a good maintaining material because it has excellent interaction with metal, chemical inert structure and easy to produce various forms and porosity [158]. The metal catalysts distributed on the carbon support are mostly employed in the hydrolysis of AB. Lu et al. [146] prepared ultrafine homogeneous Ru nanoparticles on phosphorus-doped carbon (PPC) carriers to synthesize Ru/PPC catalyst through in-situ reduction method. Figure 16 illustrated procedure for preparing of PPC and Ru<sup>3+</sup>/PPC. The Ru/PPC material could be utilized as catalyst to promote the hydrolysis of AB to produce hydrogen. In order to investigate the effect of Ru loading on the property of Ru/PPC catalyst, the hydrolysis of AB was carried out with different Ru content (1.5, 2.5, 3.5, 4.5 wt%) at 25 °C by maintaining the total concentration of Ru at 0.7 mM. It could be seen from the experimental results that Ru/PPC with a load of 3.5 wt% displayed the highest catalytic capacity with TOF value of 413 mol H<sub>2</sub> (mol<sub>Ru</sub> min)<sup>-1</sup>. Ru concentration also affected the performance of the catalyst. With the increased of Ru concentration (between 0.3 and 0.9 mM), the hydrogen production rate was increasing gradually. The high activity of AB hydrolysis on Ru/PPC was attributed to the super refinement and high dispersion of Ru NCS, which provided more surface active centers for the reaction. This review showed that the PPC had promising catalyst support for hydrogen generation from AB hydrolysis.

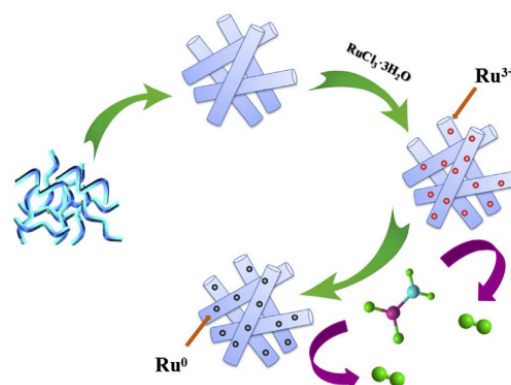


**Figure 16.** The procedure for preparing Ru<sup>3+</sup>/PPC and the hydrolysis of AB over Ru/PPC; copyright (2018), Hydrogen Energy.

On the other side, the performance of surface charge distribution and energy storage/release can be regulated and ameliorated by doped miscellaneous elements [159]. The catalyst of porous carbon material containing B, N, P heteroatoms reveal excellent catalytic performance in AB hydrolysis reaction [160,161]. So far, the method of doping nitrogen or phosphorus in carbon materials is that additional N or P sources ( $\text{NH}_3$ ,  $\text{PH}_3$ ) are required during the material preparation process [162]. The existing preparation process is cumbersome and dangerous to a certain extent, and it is rare to obtain N, P co-doped nanoporous carbon directly from existing and frequently used materials. Therefore, it is a challenge to develop a practical, valid and single technique for preparing multi-element doped (such as N, P) nanoporous carbon. Herein, Fan et al. [163] explored a simple and effective method for preparing N, P-doped nanocarbon as metal nanoparticles (MNP), in which N or P doped carbon as MNP carrier enhanced the catalytic activity of AB decomposition. They chose adenosine triphosphate (ATP) as the ideal material for N-rich and P-rich raw materials due to the high content of N and P provided by an adenine structure and three phosphate groups. Consequently, they utilized ATP-derived N, P co-doped carbon materials to fix Rh NPs in porous carbon for the catalytic dehydrogenation of AB. As shown in Figure 17, ATP-C was prepared from ATP via a one-step heat treatment procedure. ATP-C-700, ATP-C-800, ATP-C-900 were synthesized to explore the effect of temperature on surface area and pore size. It was worth mentioning that the specific surface area and average pore diameter of ATP-C-800 were the largest,  $154.2 \text{ m}^2 \text{ g}^{-1}$  and  $6.83 \text{ nm}$ , respectively. According to the above results,  $800 \text{ }^\circ\text{C}$  was taken for the optimal carbonization temperature. The TOF of Rh/ATP-C-800 catalyst hydrolyzing AB at  $25 \text{ }^\circ\text{C}$  was  $566 \text{ mol H}_2 \text{ min}^{-1} (\text{mol Rh})^{-1}$ , which was higher than that of Rh based catalyst reported in most reports [164–166]. This proves the fact that the surface metal atoms and heteroatoms are connected to each other, and the carbon material doped with heteroatoms will change the catalytic performance of the catalyst, thereby increasing the dehydrogenation rate. [167]. Thus, they speculated that the role of ATP-C enrichment of N and P atoms not only disperses Rh NPs and resides in the aggregation of metal NP, but also makes Rh NP have more accessible surface active sites.

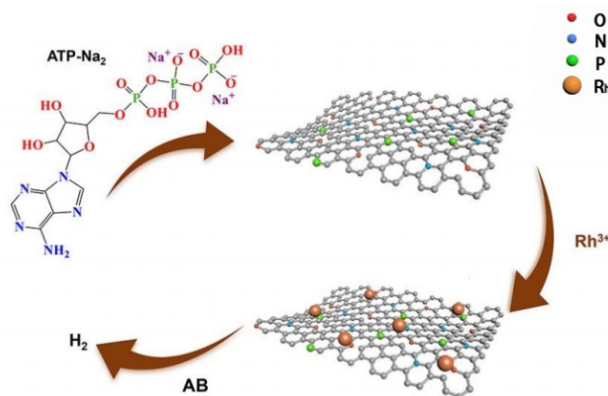


**Figure 17.** Illustration of the synthesis process of Rh/ATP-C; copyright (2020), Nanoscale Advances.

Carbon dots (CDs) has various structures, low price, easy doping (including N, B, s, P, etc.) and non-toxic. CDs are called excellent catalyst supports due to their special electron transfer properties and high specific surface area [168]. Their surfaces have many catalytically favorable positions and can support a variety of surface functional groups (such as  $-\text{NH}_2$ ,  $-\text{OH}$  and  $-\text{COOH}$ ). CDs doped with heteroatoms are conducive to adsorb hydrogen intermediates through transforming the electronic structure of the catalytically active center [169]. It is essential to promote catalytic performance, that is, by accelerating the intermolecular electron transfer to enhance the influence of the interaction between multi-component nanostructures. Lu et al. [170] prepared  $\text{RuP}_2$  nanoparticles doped with nitrogen CDs as a catalyst for AB hydrolysis reaction, called  $\text{RuP}_2/\text{CDs}$ . The  $\text{RuP}_2/\text{CDs}$  nanocomposites were successfully prepared by simple physical mixing of CDs, phytic acid and ruthenium ions. Figure 18 illustrated the preparation process of  $\text{RuP}_2/\text{CDs}$  nanocomposites. In view of characterization

and testing of catalytic performance, a simple synergistic mechanism could roughly explain the catalytic performance of this composite material. Firstly, AB molecules were adsorbed on RuP<sub>2</sub> NPs, which activated the breaking of B-H and O-H bonds; secondly, adjacent C and N atoms could simultaneously activate water to promote the transfer of protons from RuP<sub>2</sub> to the water inside the carbon nanosheets. The mechanism of hydrogen production by AB was that the dissociated H atoms in the B-H bond of AB molecules could combine with protonated water molecules to form hydrogen molecules. RuP<sub>2</sub> NPs and nitrogen-doped CDs could act as bifunctional active sites, activating AB and water molecules, thus, significantly accelerating the release of hydrogen. In addition, the nanosheets morphology of CDs further increased the catalytic activity of hydrogen production by strengthening the utilization rate of active centers.

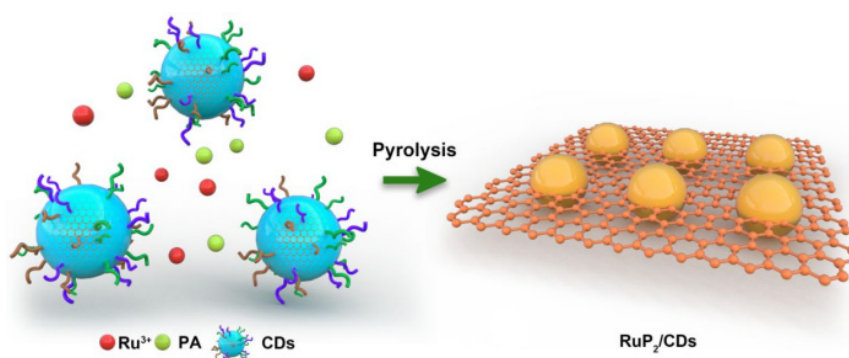


**Figure 18.** Illustration of the synthesis of the RuP<sub>2</sub>/carbon dots (CDs) nanocomposites; copyright 2020, American Chemical Society.

### 3.3.3. Carbon Nanotubes Material Supported Metal Catalysts

CNT is a new kind of honeycomb lattice graphene layer, whose outer diameter ranges from 1 to 100 nm [171]. According to the number of graphene layers, carbon nanotubes can be single-wall (SWCNT) and multi-wall (MWCNT) [172]. Carbon nanotubes are very attractive as catalyst carriers because they have a high surface area and provide a high proportion of nanoparticles. Moreover, the contact surface between the reactant and the active region is greatly increased [173]. Their mesoporous structure is suitable for increasing the mass transfer rate between the reactant and the active center, so it has a significant impact on the catalytic activity [174].

Recently, except for engineering the surface chemistry of CNT support, adding surface ligands could be another potential strategy to engineer metal electronic properties owing to its flexible capacity for demand of stability [60]. Along this line, Fu W et al. [175] proposed a new strategy to engineer the surface of catalysts and electronic properties of Pt/CNT using polyoxometalates (POMs) as the ligands in 2019. They designed three types of POMs including silicotungstic acid (STA), phosphotungstic acid (PTA) and molybdphosphoric acid (PMA), respectively, which were established and analyzed by a combination of kinetic and isotopic analyses with various characterization techniques. It could be obviously showed in Figure 19 that the rate of hydrogen generation was extremely sensitive to the kinds of POMs following the order of STA-Pt/CNT > PTA-Pt/CNT > Pt/CNT > PMA-Pt/CNT, with the STA-Pt/CNT having the highest rate of production hydrogen, which indicated the promotion effects of STA on the catalytic reaction. According to all characterization techniques, the analytic results indicated that the STA compared to the PTA and the PMA acted as a good receptor to increase the binding energy of Pt in order to improve hydrogen production efficiency and catalyst durability. From these experiment consequences, choosing POMs based on their electron-absorbing/donating properties was of vital importance to adjust the electronic nature of catalysts.

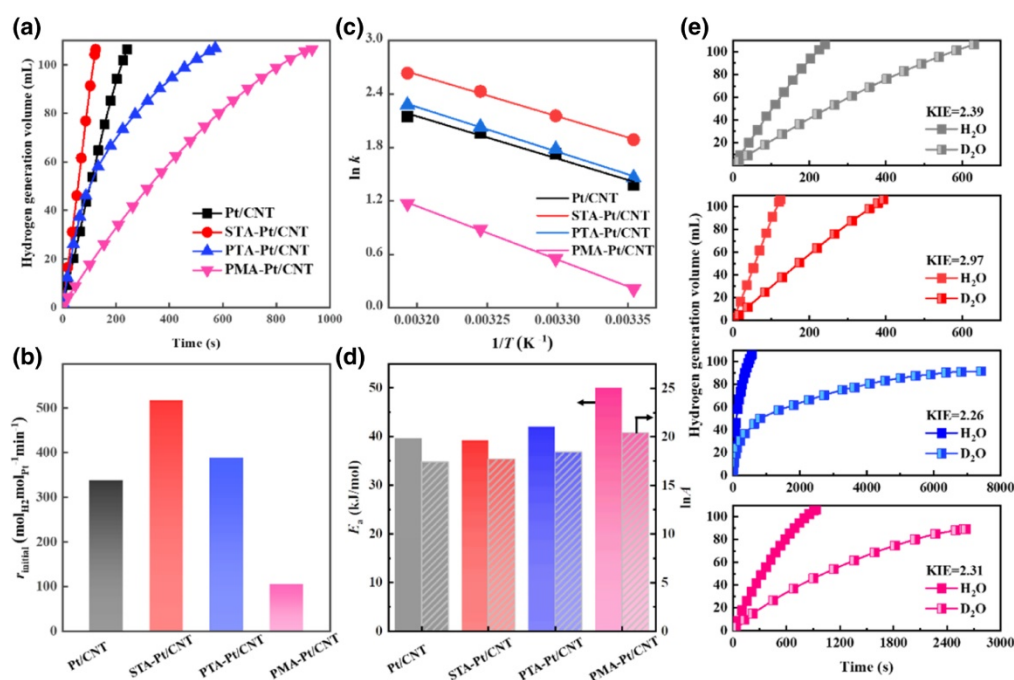


**Figure 19.** (a) Hydrogen generation volume as a function of time; (b) the initial hydrogen generation rate ( $r_{\text{initial}}$ ) over Pt/CNT, silicotungstic acid (STA)-Pt/CNT, phosphotungstic acid (PTA)-Pt/CNT and molybdphosphoric acid (PMA)-Pt/CNT catalysts. Reaction conditions: 30 °C,  $n_{\text{Pt}} : n_{\text{AB}} : n_{\text{W/Mo}} = 1:420:40$ ,  $m_{\text{cat}} = 0.025$  g,  $c_{\text{AB}} = 0.01\text{g mL}^{-1}$ ; (c)  $\ln k$  as a function of  $1/T$ ; (d) the corresponding activation energy ( $E_a$ ) and the logarithm of pre-exponential factor ( $\ln A$ ); (e) hydrogen generation volume as a function of time at 30 °C over the four catalysts using  $\text{H}_2\text{O}$  or  $\text{D}_2\text{O}$  as the reactant; copyright (2020), Journal of Energy Chemistry.

Akbayrak S et al. [173] reported the in situ formation of ruthenium (0) nanoparticles supported on MWCNT catalyst during AB hydrolysis at room temperature. Ru (III) ions were impregnated on MWCNT surface from aqueous solution of Ru(III) chloride, and then reduced by AB to form multi walled carbon nanotubes, referred to as Ru(0)@MWCNT. The results showed that Ru nanoparticles were well dispersed on the walls of carbon nanotubes in the range of 2.0–3.0 nm. They used Ru(III)@MWCNT sample with various Ru loading (0.73, 1.47, 1.91, 2.26, 2.83 wt%) to provide the same ruthenium concentration. The catalytic activity of Ru(0)@MWCNT with Ru loading of 1.91 wt% Ru was the highest at 25 °C. As the further increase of Ru loading, the catalytic activity of Ru(0)@MWCNT decreases, which was probably due to the agglomeration of nanoparticles, resulting in the decrease of specific surface area and accessibility of active sites. It was expected that the catalytic activity of Ru(0)@MWCNTs was still 41% of its initial catalytic activity even after the fourth operation. The easy preparation and high catalytic performance of Ru(0)@MWCNT revealed that the Ru(0)nanoparticle catalyst supported on MWCNTs was a promising catalyst for the development of efficient and portable hydrogen production system.

### 3.3.4. Silicon Dioxide Material Supported Metal Catalysts

In recent years, metal nanoparticles in porous silica shell have attracted people's attention because of the possibility of obtaining nano scale monodisperse particles [176]. The obtained core-shell structure can fully prevent the aggregation of metal nanoparticles through the protection of porous silica shell, so as to improve the stability of metal nanoparticles and the long-term use performance of metal nanoparticles [143].

The core-shell metal NPs not only have the characteristic of heterogeneous metals, but also present distinct chemical and physical performances [177,178]. Moreover, it is particularly noted that

a one-pot reduction technology is indeed required to prepare the core-shell heterometallic catalyst. Hu J et al. [148] reported a one-pot synthesis of core-shell-type nanospheres Pt@SiO<sub>2</sub>, which displayed excellent stability and performance after recycle test for hydrogen generation from AB at room temperature. The detailed measurement and characterization of the nanoparticles were carried out through SEM and TEM techniques. As shown in Figure 20a, The SEM image shown that the average diameter of the prepared Pt@SiO<sub>2</sub> was 25 nm, and the particle size was uniform. The monodisperse spherical morphology of Pt@SiO<sub>2</sub> could make further efforts to be affirmed by TEM images. It was found in Figure 20b that a single Pt NP as a core with a diameter of 4 nm was available embedded in the silica nanospheres. Pt@SiO<sub>2</sub> NPs and Pt/SiO<sub>2</sub> were investigated for their catalytic activity in AB hydrolysis at room temperature. The results were shown in Figure 21a that the hydrogen precipitation was completed in 7.72, 55.98 and 111, in existence of as-synthesized Pt@SiO<sub>2</sub>, Pt/SiO<sub>2</sub> and Pt Nps, respectively. Moreover, the hydrogen production rate of AB was Pt@SiO<sub>2</sub> > Pt/SiO<sub>2</sub> > Pt > SiO<sub>2</sub>. Among all the catalysts, Pt@SiO<sub>2</sub> emerged the highest catalytic activity for generation hydrogen in AB aqueous solution while the TOF value can reach 158.6 mol H<sub>2</sub> (mol Pt min)<sup>-1</sup>. Compared with other core-shell catalysts, Pt-based nanocatalysts had higher catalytic activity in the same reaction. In the whole reaction process, after five times of operation, the catalytic activity of Pt@SiO<sub>2</sub> NPs catalyst did not decrease significantly owing to the metal core covered by the silicon shell as Figure 21b shown, which exhibited the excellent stability of the nucleocapsid structure catalyst. In NP-5/cyclohexane reverse micelle system, Ru@SiO<sub>2</sub> core-shell nanospheres were successfully prepared [69]. The results of TEM and EDX exhibited that with the increase of Ru loading, the amount of RuNP in SiO<sub>2</sub> spherical particles increased. At room temperature, the synthesized Ru@SiO<sub>2</sub> catalyst had excellent catalytic activity and good durability for the aqueous solution of the AB. The activation energy of Ru@SiO<sub>2</sub> was estimated to be about 38.2 KJ/mol, which was lower than that of many different Ru-based and other noble metal catalysts for the hydrolysis of AB, indicating that these core-shell nanospheres had excellent catalytic performance.

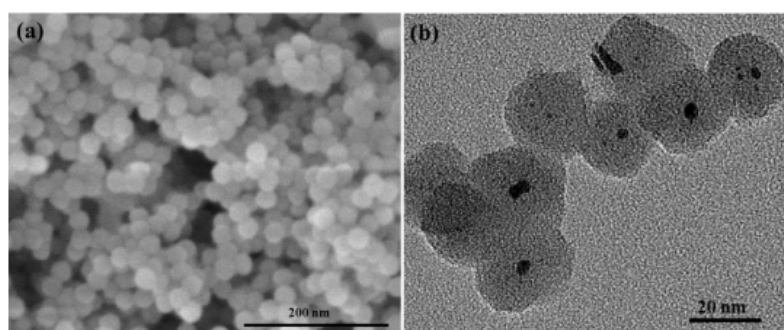


Figure 20. (a) SEM, (b) TEM images of Pt@SiO<sub>2</sub>; copyright (2015), Elsevier.

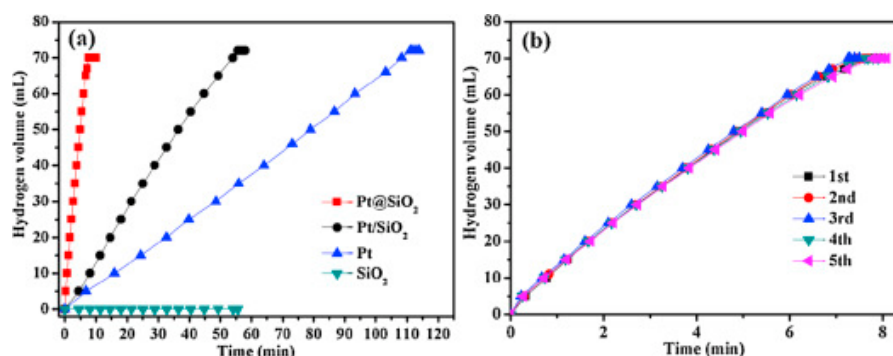
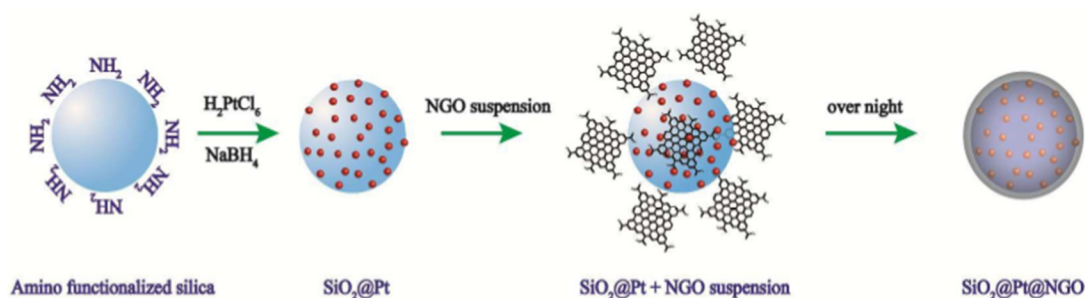


Figure 21. (a) Plots of the volume of hydrogen generation from AB (100 mM, 10 mL) hydrolysis as a function of time catalyzed by Pt@SiO<sub>2</sub>, Pt/SiO<sub>2</sub>, Pt and SiO<sub>2</sub> at 25 °C, respectively; (b) recyclability of Pt@SiO<sub>2</sub>; copyright (2015), Elsevier.

Platinum based catalysts have attracted considerable attention according to higher hydrogen generation activities among the transition metal catalysts [179]. Ye et al. [180] synthesized a supported catalyst  $\text{SiO}_2\text{@Pt@NGO}$ , in which nanometer graphene oxidem (NGO) was coated with a layer of 1 nm and the average size of the supported Pt nanoparticles was 1.9 nm (Figure 22). Through the experimental comparative analysis, the activity and stability of AB hydrolyzed hydrogen production would be improved by the increased content of NGO. The enhanced catalytic performance of  $\text{SiO}_2\text{@Pt@NGO}$  could be attributed to the synergistic effects among NGO, Pt nanoparticles and  $\text{SiO}_2$ , especially the modified electronic structure of Pt nanoparticles by NGO coating.



**Figure 22.** Illustration of the formation process of  $\text{SiO}_2\text{@Pt@NGO}$ ; copyright (2017), Sustainable Energy and Fuels.

### 3.3.5. Cerium Dioxide Material Supported Metal Catalysts

Transition metal nanoparticles tend to aggregate to larger particles, which eventually lead to shorter lifetime. However, reducible oxide supports such as cerium ( $\text{CeO}_2$ ) combined with metal nanoparticles have high activity in many reactions [181–183]. Cerium oxide has cerium (III) defect, which is easy to form due to its favorable large positive reduction potential of  $\text{Ce}^{4+} \rightarrow \text{Ce}^{3+}$  (1.76 V [184] in acid solution). Under the catalytic reaction conditions, the two oxidation states of cerium(IV) and cerium(III) can be mutually converted, that is, cerium oxide can be redox cycled in an aqueous solution [185]. The formation of cerium(III) causes excessive negative charges to accumulate on the surface of the oxide, which enhances the coordination between metal(0) nanoparticles and the oxide surface, thus enhancing the catalytic activity through more favorable substrate metal interaction [186]. Therefore, ceria has been used to improve the catalytic performance of transition metals through strong metal-support interactions, especially electron-rich post-transition metal nanoparticles [187–189]. Therefore, more and more attention has been paid to cerium as a support material to stabilize the anti-aggregation of metal nanoparticles. Tonbul's group [149] reported the preparation, characterization and catalytic application of palladium(0) nanoparticles supported on cerium,  $\text{Pd}^0/\text{CeO}_2$ . Palladium(II) ion impregnated on the surface of nanospheres with an average particle size of 25 nm were reduced to  $\text{Pd}^0/\text{CeO}_2$  by sodium borohydride, which was used as a catalyst for hydrogen generation from the hydrolysis of AB [190]. The high catalytic activity of  $\text{Pd}^0/\text{CeO}_2$  was attributed to the reducibility of cerium, that is to say, two kinds of cerium(IV) and cerium(III) transformed each other under catalytic reaction. The formation of cerium(III) led to the accumulation of excessive negative charges on the oxidation surface, which enhanced the ligand interaction between the metal nanoparticles and the oxidation surface.  $\text{Pd}^0/\text{CeO}_2$  samples with Palladium loading capacity of 1.18 wt% exhibited the highest activity in AB hydrolysis at room temperature.

Özkar et al. [70] prepared rhodium (0) nanocatalyst with cerium ( $\text{CeO}_2$ ), silicon ( $\text{SiO}_2$ ), alumina ( $\text{Al}_2\text{O}_3$ ), titanium ( $\text{TiO}_2$ ), zirconia ( $\text{ZrO}_2$ ) and hafnium ( $\text{HfO}_2$ ) as carriers for the hydrolysis of AB under the same conditions, and then investigated the influence of various oxygenate carriers on the catalytic activity of rhodium boron nanoparticles in the hydrogen produced by AB hydrolysis. It was easy to see from the figure description in Figure 23 that in the tested catalyst, rhodium (0) nanoparticles supported on nanoceria revealed the highest catalytic activity in the hydrogen produced by the hydrolysis of AB at room temperature. The resulting  $\text{Rh}^0/\text{CeO}_2$  with a metal loading of 0.1 wt% Rh had excellent catalytic

activity for the hydrogen production from hydrolysis of AB with TOF of  $2010 \text{ min}^{-1}$ .  $\text{Rh}^0/\text{CeO}_2$  was a reusable catalyst that retained 67% of its initial catalytic activity, even after the fifth use of hydrogen produced by the hydrolysis of AB at room temperature (TOF = 1350).  $\text{Rh}^0/\text{CeO}_2$  was a very attractive catalyst for hydrogen generation due to its simple preparation and high catalytic activity as a solid hydrogen storage material.

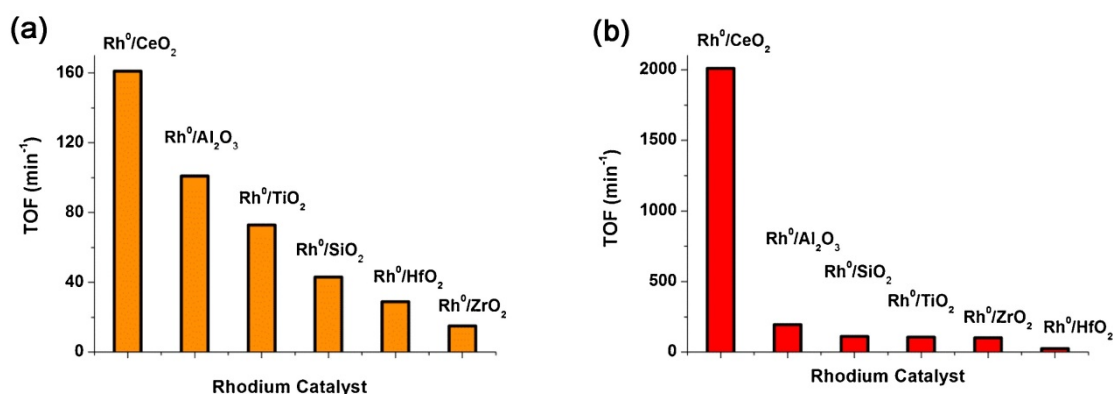


**Figure 23.** Comparison of TOF (turnover frequency in  $\text{mol H}_2/(\text{mol Rh} \times \text{min})$ ) values of rhodium nanoparticles supported on different oxides at (a) high and (b) low rhodium loadings of catalysts used in hydrogen generation from the hydrolysis of ammonia borane (10 mL, 100 mM) at  $25.0^\circ\text{C}$ ; copyright (2016), Elsevier.

Heterogeneous catalytic liquid phase selective hydrogenation is widely used in chemical synthesis in industry. However, active nanoparticles (such as Pd) have high conversion and selectivity, especially under mild conditions, while preventing aggregation/leaching [191]. Li et al. [192] prepared  $\text{CeO}_2$  nanotubes/Pd@MIL-53 (Al) sandwich structure catalyst to solve these problems, in which MIL-53 (Al) porous shell can effectively stabilize Pd nanoparticles. The  $\text{CeO}_2$  nanotubes/million Pd-53(Al) were synthesized under mild conditions without any surfactant or carrier surface modification, as shown in Figure 24. Compared with  $\text{CeO}_2$  nanotubes/Pd and Pd/MIL-53 (Al), due to the promotion effect of  $\text{CeO}_2$  and the enrichment/sieving effect of MIL-53(Al),  $\text{CeO}_2$  nanotubes/Pd@MIL-53(Al) exhibited the highest catalytic performance in terms of conversion rate and selectivity.

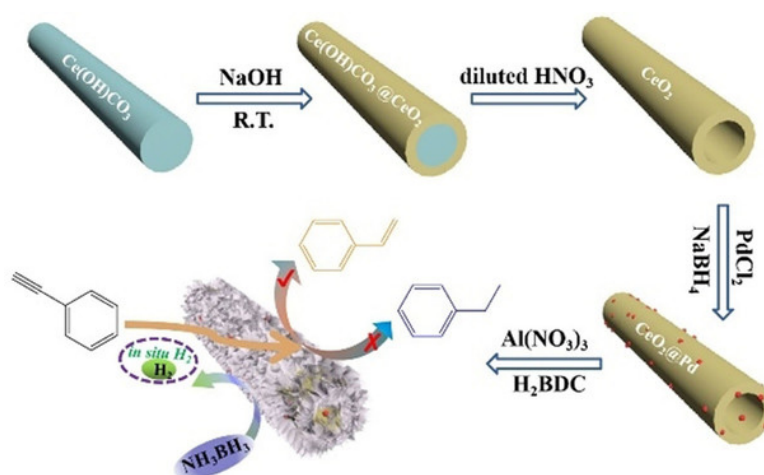


**Figure 24.** Illustration of the formation of  $\text{CeO}_2$  nanotube/Pd@MIL-53(Al); copyright 2020, Wiley.

### 3.3.6. Titanium Dioxide Material Supported Metal Catalysts

The specific surface area of porous titanium dioxide is between  $10\text{--}300 \text{ m}^2/\text{g}$ , which can be used as a carrier to avoid the diffusion problem in porous materials [193]. In recent years, people pay more

and more attention to the research of titanium dioxide as precious metal carrier material, because its chemical stability, interesting optical, antibacterial and catalytic properties, titanium dioxide has been widely used in the fields of filler, catalyst carriers and photocatalysts [194,195].

Akbayrak S et al. [150] reported that nanotitanium supported ruthenium (0) nanoparticles as catalysts for AB hydrolysis to produce hydrogen. Ru(0)/TiO<sub>2</sub> exhibited high catalytic activity in hydrogen generation from the hydrolysis of AB its TOF value showing as high as 241 min<sup>-1</sup> at room temperature. This catalytic activity was due to the dispersion of small nanoparticles on the large outer surface of TiO<sub>2</sub> nanoparticles. Ru(0)/TiO<sub>2</sub> was reusable catalysts, because it provided complete hydrolysis of AB generating three mol H<sub>2</sub> per mole of AB in the third run, but the catalytic activity had no significant change. Furthermore, Ru(0)/TiO<sub>2</sub> was a long-life catalyst, which could provide 71,500 cycles of hydrogen production by hydrolysis of AB at 25.0 °C. M. Rakap et al. [196] prepared Pd-activated TiO<sub>2</sub>-supported Co-Ni-P ternary alloy catalyst (Co-Ni-P/Pd-TiO<sub>2</sub>) by chemical deposition method. Cobalt based catalysts were more active and expensive than nickel based catalysts in the hydrolysis of AB. In order to obtain a cheap catalyst with activity around the pure cobalt catalyst, they prepared alloy catalysts by changing the cobalt nickel ratio, and tested their catalytic activity in AB hydrolysis. Figure 25 showed that there are alloy type catalysts with different cobalt nickel ratio in the time curve of hydrogen volume generated by hydrolysis of AB solution. As seen from Figure 26, Co-Ni-P/Pd-TiO<sub>2</sub> catalyst revealed good durability in recycling. Even in the fifth cycle, it exhibited the same catalytic activity as the first cycle. Co-Ni-P/Pd-TiO<sub>2</sub> catalyst had the advantages of high efficiency, low cost and reusability, which made them a promising candidate in the hydrolysis of AB to produce hydrogen.

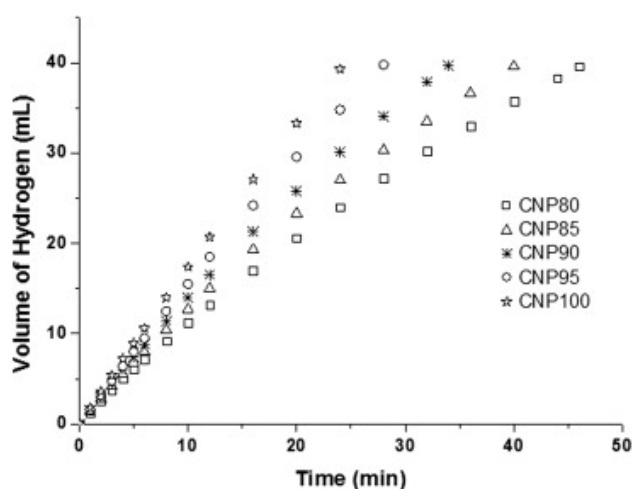


**Figure 25.** Plot of the volume of H<sub>2</sub> (mL) versus time (min) for the hydrolysis of AB (31.8 mg, 50 mM) catalyzed by Co-Ni-P/Pd-TiO<sub>2</sub> catalysts (25 mg) with different compositions; copyright (2010), Hydrogen Energy.

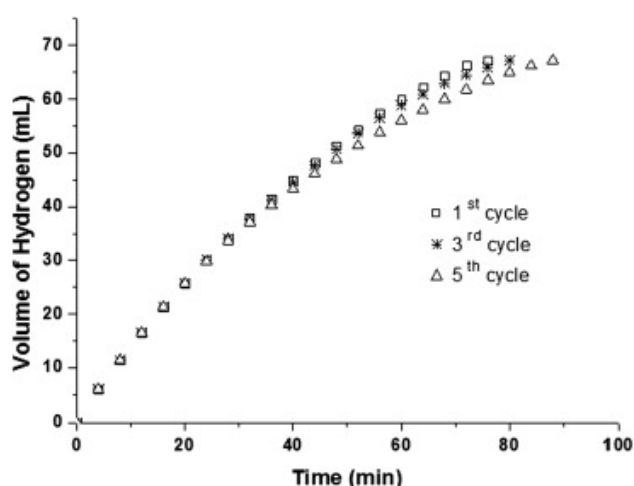


**Figure 26.** Reusability tests of the Co-Ni-P/Pd-TiO<sub>2</sub> catalyst in the hydrolysis AB (31.8 mg, 50 mM); copyright (2010), Hydrogen Energy.

#### 4. Direction of Development

Ammonia borane is a potential candidate material owing to its unique properties, which has the advantages of high theoretical hydrogen capacity, good solubility, stability, environmental safety, etc. The aqueous solution of AB is very stable at room temperature, but in the presence of a metal catalyst, AB can quickly liberate hydrogen from water. The catalysts for AB hydrolytic dehydrogenation are principally transition metal nanoparticles, including noble metal and non-precious metal catalysts. The noble metals are mainly Pd, Pt, Ru, Rh, while the non-precious are mainly Cu, Fe, Ni and Co.

Noble metals have always displayed outstanding catalytic performance in the catalytic hydrolysis of AB on the basis of existing literature reviews. However, in the practical application, due to the limited precious metal resources and high price, the cost of hydrogen production keeps increasing, which limits the mass production and application of noble metals. In terms of non-precious metals, as abundant resources and low price transition metal, have also been experimentally attested certain level of catalytic capacity for dehydrogenation of AB [197,198]. It has been proved by many related studies that the performance of the catalyst is largely determined by the phase composition, microstructure and surface morphology of the bimetallic or multimetallic catalyst [199–201]. The coordination of electron configuration and geometry among metal components and the effective coordination can make the bimetal or polymetal composites with stronger catalytic capacity [202–205]. In order to highlight the advantages of noble metals and non-precious metals, we reviewed the bimetallic or polymetallic composite catalysts formed by noble metals and non-precious metals. Therefore, the low-cost and effective catalysts composed of precious metals and non-noble metals are worthy of expectation and further intensive study [102]. In addition, we also explore the catalytic effect of noble metal catalysts supported on various support materials for AB hydrolysis. It was found that the supported catalysts can significantly increase the rate of hydrogen evolution under the support of the carriers. Therefore, it is particularly important to find and investigate suitable carriers.

On the other hand, the lattice irregularity is closely related to the catalytic activity and the metal surface properties such as chemisorption and electron transfer. To make ammonia borane hydrogen production widely used, the efficient catalyst can be explored from the aspects of adjusting the degree of chemisorption and electron transfer between catalyst and molecule of AB. It is believed that with the continuous efforts of researchers, metal-catalyzed hydrogen production from AB will be more and more in practical applications.

At present, the biggest challenge in the research of AB hydrogen storage is how to realize efficient regeneration and recycling. Although some evolution has been developed in allusion to recycling of AB from the by-products of pyrolysis, alcoholysis and hydrolytic dehydrogenation, respectively, in this

regard, the regeneration yield of AB still needs to be further improved and studied. Compared with the large number of studies on the decomposition of AB to produce hydrogen, there are few studies on the regeneration of AB. Therefore, the regeneration of AB will be the key research direction in the future. In addition, the current market price of ab is relatively expensive, so it is significant to develop a technology suitable for large-scale industrial production of AB in the future, so as to effectively reduce the cost of using AB as hydrogen storage material.

## 5. Conclusions

Currently, with the continuous progress of science and technology, the consumption of fossil energy causes a serious of environmental problems, thus the development of efficient and clean energy has attracted more and more attention to replace traditional fuels. Hydrogen, as an ideal energy carrier, plays the main representatives role in the field of future new energy. Ammonia Borane, being not only hydrogen storage but hydrogen production, is considered as a potential hydrogen storage material on account of its high theoretical hydrogen content, environmental friendliness, good cycling performance and excellent stability. We analyzed and compared the advantages and disadvantages of three AB decomposition methods, including pyrolysis, alcoholysis and hydrolysis. In these ways of producing hydrogen, compared with alcoholysis, producing many by-products, and pyrolysis under the high temperature condition, hydrolysis has obvious advantages. Nowadays, the research on the hydrolysis of AB primarily focuses on the synthesis of simple catalysts with high stability and good cycling ability, which provides the possibility for the practical application of AB. Furthermore, we explored the effects of using carbon, graphene, carbon nanotubes (CNT), silica, ceria and titanium supported catalysts on the hydrolytic dehydrogenation of AB. Simultaneously, the activity, reusability and turnover frequency (TOF) value of these catalysts for AB dehydrogenation reaction were introduced, and the future development prospects of precious metal catalysts were prospected.

**Author Contributions:** Conceptualization, C.W. and X.L.; writing—original draft preparation, M.L., L.Z., and X.L.; writing—review and editing, M.L., X.L. and L.X.; supervision, C.W. All authors have read and agreed to the published version of the manuscript.

**Funding:** This research was supported by Anhui Provincial Natural Science Foundation (1908085QB68), the Natural Science Foundation of the Anhui Higher Education Institutions of China (KJ2019A0072), the Major Science and Technology Project of Anhui Province (201903a05020055), the Foundation of Zhejiang Provincial Key Laboratory of Advanced Chemical Engineering Manufacture Technology (ZJKL-ACEMT-1802), the China Postdoctoral Science Foundation (2019M662060), and the Research Fund for Young Teachers of Anhui University of Technology (QZ201610).

**Conflicts of Interest:** The authors declare no conflicts of interest.

## References

1. Adeniran, B.; Mokaya, R. Compaction: A mechanochemical approach to carbons with superior porosity and exceptional performance for hydrogen and CO<sub>2</sub> storage. *Nano Energy* **2015**, *16*, 173–185. [[CrossRef](#)]
2. Zhou, L.; Sun, L.; Xu, L.X.; Wan, C.; An, Y.; Ye, M.F. Recent Developments of Effective Catalysts for Hydrogen Storage Technology Using N-Ethylcarbazole. *Catalysts* **2020**, *10*, 648. [[CrossRef](#)]
3. Zhu, Q.L.; Xu, Q. Liquid organic and inorganic chemical hydrides for high-capacity hydrogen storage. *Energy Environ. Sci.* **2015**, *8*, 478–512.
4. Niaz, S.; Manzoor, T.; Pandith, A.H. Hydrogen storage: Materials, methods and perspectives. *Renew. Sustain. Energy Rev.* **2015**, *50*, 457–469. [[CrossRef](#)]
5. Ali, N.; Hussain, A.; Ahmed, R.; Wang, M.K.; Zhao, C.; Haq, B.U.; Fu, Y.Q. Advances in nanostructured thin film materials for solar cell applications. *Renew. Sustain. Energy Rev.* **2016**, *59*, 726–737. [[CrossRef](#)]
6. Wan, C.; Zhou, L.; Sun, L.; Xu, L.X.; Cheng, D.G.; Chen, F.Q.; Zhan, X.L.; Yang, Y.R. Boosting visible-light-driven hydrogen evolution from formic acid over AgPd/2D g-C<sub>3</sub>N<sub>4</sub> nanosheets Mott-Schottky photocatalyst. *Chem. Eng. J.* **2020**, *396*, 125229.

7. Liu, Q.B.; Zhang, S.J.; Liao, J.Y.; Feng, K.J.; Zheng, Y.Y.; Pollet, B.G.; Li, H. CuCo<sub>2</sub>O<sub>4</sub> nanoplate film as a low-cost, highly active and durable catalyst towards the hydrolytic dehydrogenation of ammonia borane for hydrogen production. *J. Power Sources* **2017**, *355*, 191–198. [[CrossRef](#)]
8. Wan, C.; Cheng, D.G.; Chen, F.Q.; Zhan, X.L. Fabrication of CeO<sub>2</sub> nanotube supported Pt catalyst encapsulated with silica for high and stable performance. *Chem. Commun.* **2015**, *51*, 9785–9788. [[CrossRef](#)]
9. Wan, C.; An, Y.; Xu, G.H.; Kong, W.J. Study of catalytic hydrogenation of N-ethylcarbazole over ruthenium catalyst. *Int. J. Hydrog. Energy* **2012**, *37*, 13092–13096. [[CrossRef](#)]
10. Wan, C.; Sun, L.; Xu, L.X.; Cheng, D.G.; Chen, F.Q.; Zhan, X.L.; Yang, Y.R. Novel NiPt alloy nanoparticle decorated 2D layered g-C<sub>3</sub>N<sub>4</sub> Nanosheets: A highly efficient catalyst for hydrogen generation from hydrous hydrazine. *J. Mater. Chem. A* **2019**, *7*, 8798–8804. [[CrossRef](#)]
11. Li, X.F.; Ma, X.F.; Zhang, J.; Akiyama, E.; Wang, Y.F.; Song, X.L. Review of Hydrogen Embrittlement in Metals: Hydrogen Diffusion, Hydrogen Characterization, Hydrogen Embrittlement Mechanism and Prevention. *Acta Metall. Sin.* **2020**, *33*, 1–15. [[CrossRef](#)]
12. Zhang, M.Y.; Liu, L.; Lu, S.; Xu, L.X.; An, Y.; Wan, C. Facile Fabrication of NiPt/CNTs as an Efficient Catalyst for Hydrogen Production from Hydrous Hydrazine. *ChemistrySelect* **2019**, *4*, 10494–10500. [[CrossRef](#)]
13. Zhu, M.; Xu, L.; Du, L.; An, Y.; Wan, C. Palladium Supported on Carbon Nanotubes as a High-Performance Catalyst for the Dehydrogenation of Dodecahydro-N-ethylcarbazole. *Catalysts* **2018**, *8*, 638. [[CrossRef](#)]
14. Attia, N.F.; Lee, S.M.; Kim, H.J.; Geckeler, K.E. Nanoporous polypyrrole: Preparation and hydrogen storage properties. *Int. J. Energy Res.* **2014**, *38*, 466–476. [[CrossRef](#)]
15. Oumellal, Y.; Courty, M.; Rougier, A.; Nazri, G.A.; Aymard, L. Electrochemical reactivity of magnesium hydride toward lithium: New synthesis route of nano-particles suitable for hydrogen storage. *Int. J. Hydrog. Energy* **2014**, *39*, 5852–5857. [[CrossRef](#)]
16. Kojima, Y. Hydrogen storage materials for hydrogen and energy carriers. *Int. J. Hydrog. Energy* **2019**, *44*, 18179–18192. [[CrossRef](#)]
17. Andersson, J.; Grönkvist, S. Large-scale storage of hydrogen. *Int. J. Hydrog. Energy* **2019**, *23*, 11901–11919. [[CrossRef](#)]
18. Yao, F.; Li, X.; Wan, C.; Xu, L.X.; An, Y.; Ye, M.F.; Lei, Z. Highly efficient hydrogen release from formic acid using a graphitic carbon nitride-supported AgPd nanoparticle catalyst. *Appl. Surf. Sci.* **2017**, *426*, 605–611. [[CrossRef](#)]
19. Semiz, L. Hydrogen generation from ammonia borane by chemically dealloyed platinum nanoparticles. *React. Kinet. Mech. Catal.* **2020**, *129*, 205–218. [[CrossRef](#)]
20. Staubitz, A.; Robertson, A.P.; Manners, L. Ammonia-borane and related compounds as dihydrogen sources. *Chem. Rev.* **2010**, *110*, 4079–4124. [[CrossRef](#)]
21. Yao, Q.L.; Lu, Z.H.; Huang, W.; Chen, X.S.; Zhu, J. High Pt-like activity of the Ni–Mo/graphene catalyst for hydrogen evolution from hydrolysis of ammonia borane. *J. Mater. Chem. A* **2016**, *4*, 8579–8583. [[CrossRef](#)]
22. Sutton, A.D.; Burrell, A.K.; Dixon, D.A.; Garner, E.B.; Gordon, J.C.; Nakagawa, T.; Ott, K.C.; Robinson, P.; Vasiliu, M. Regeneration of ammonia borane spent fuel by direct reaction with hydrazine and liquid ammonia. *Science* **2011**, *331*, 1426–1429. [[CrossRef](#)]
23. Smythe, N.C.; Gordon, J.C. Ammonia borane as a hydrogen carrier: Dehydrogenation and regeneration. *Eur. J. Inorg. Chem.* **2010**, 509–521. [[CrossRef](#)]
24. Sun, Q.M.; Wang, N.; Bai, R.S.; Hui, Y.; Zhang, T.J.; Do, D.A.; Zhang, P.; Song, L.J.; Miao, S.; Yu, J.H. Synergetic Effect of Ultrasmall Metal Clusters and Zeolites Promoting Hydrogen Generation. *Adv. Sci.* **2019**, *6*, 1802350. [[CrossRef](#)]
25. Amali, A.J.; Aranishi, K.; Uchida, T.; Xu, Q. PdPt Nanocubes: A High-Performance Catalyst for Hydrolytic Dehydrogenation of Ammonia Borane. *Part. Part. Syst. Character.* **2013**, *30*, 888–892. [[CrossRef](#)]
26. Roy, B.; Hajari, A.; Kumar, V.; Manna, J.; Sharma, P. Kinetic model analysis and mechanistic correlation of ammonia borane thermolysis under dynamic heating conditions. *Int. J. Hydrog. Energy* **2018**, *43*, 10386–10395. [[CrossRef](#)]
27. Yan, J.M.; Zhang, X.B.; Shioyama, H.; Xu, Q. Room temperature hydrolytic dehydrogenation of ammonia borane catalyzed by Co nanoparticles. *J. Power Sources* **2010**, *195*, 1091–1094. [[CrossRef](#)]
28. Chandra, M.; Xu, Q. A high-performance hydrogen generation system: Transition metal-catalyzed dissociation and hydrolysis of ammonia-borane. *J. Power Sources* **2006**, *156*, 190–194. [[CrossRef](#)]

29. Sun, D.H.; Mazumder, V.; Metin, O.; Sun, S.H. Hethanolysis of ammonia borane by CoPd nanoparticles. *ACS Catal.* **2012**, *2*, 1290–1295. [[CrossRef](#)]
30. Marder, T.B. Will we soon be fueling our automobiles with ammonia–borane? *Angew. Chem. Int. Ed.* **2007**, *46*, 8116–8118. [[CrossRef](#)]
31. Gutowska, A.; Li, L.Y.; Shin, Y.S.; Wang, C.M.; Li, X.H.; Linehan, J.C.; Smith, R.S.; Kay, B.D.; Schmid, B.; Shaw, W.; et al. Nanoscaffold mediates hydrogen release and the reactivity of ammonia borane. *Angew. Chem. Int. Ed.* **2005**, *44*, 3578–3582. [[CrossRef](#)]
32. Li, Z.Y.; Zhu, G.Z.; Lu, G.Q.; Qiu, S.L.; Yao, X.D. Ammonia borane confined by a metal– organic framework for chemical hydrogen storage: Enhancing kinetics and eliminating ammonia. *J. Am. Chem. Soc.* **2010**, *132*, 1490–1491. [[CrossRef](#)] [[PubMed](#)]
33. Stephens, F.H.; Baker, R.T.; Matus, M.H.; Grant, D.J.; Dixon, D.A. Acid initiation of ammonia–borane dehydrogenation for hydrogen storage. *Angew. Chem. Int. Ed.* **2007**, *46*, 746–749. [[CrossRef](#)] [[PubMed](#)]
34. Wang, L.B.; Li, H.L.; Zhang, W.B.; Zhao, X.; Qiu, J.X.; Li, A.W.; Zheng, X.S.; Hu, Z.P.; Si, R.; Zeng, J. Supported rhodium catalysts for ammonia–borane hydrolysis: Dependence of the catalytic activity on the highest occupied state of the single rhodium atoms. *Angew. Chem. Int. Ed.* **2017**, *56*, 4712–4718. [[CrossRef](#)]
35. Hamilton, C.W.; Baker, R.T.; Staubitz, A.; Manners, I. B–N compounds for chemical hydrogen storage. *Chem. Soc. Rev.* **2009**, *38*, 279–293. [[CrossRef](#)]
36. Diwan, M.; Diakov, V.; Shafirovich, E.; Varma, A. Noncatalytic hydrothermolysis of ammonia borane. *Int. J. Hydrog. Energy* **2008**, *33*, 1135–1141. [[CrossRef](#)]
37. Diwan, M.; Hanna, D.; Varma, A. Method to release hydrogen from ammonia borane for portable fuel cell applications. *Int. J. Hydrog. Energy* **2010**, *35*, 577–584. [[CrossRef](#)]
38. Demirci, U.B.; Akdim, O.; Miele, P. Ten-year efforts and a no-go recommendation for sodium borohydride for on-board automotive hydrogen storage. *Int. J. Hydrog. Energy* **2009**, *34*, 2638–2645. [[CrossRef](#)]
39. Hu, M.G.; Geanangel, R.A.; Wendlandt, W.W. The thermal decomposition of ammonia borane. *Thermochim. Acta* **1978**, *23*, 249–255. [[CrossRef](#)]
40. Nakagawa, Y.; Ikarashi, Y.; Isobe, S.; Hino, S.; Ohnuki, S. Ammonia borane–metal alanate composites: Hydrogen desorption properties and decomposition processes. *RSC Adv.* **2014**, *4*, 20626–20631. [[CrossRef](#)]
41. Dong, H.L.; Berke, H. A mild and efficient rhenium-catalyzed transfer hydrogenation of terminal olefins using alcoholysis of amine–borane adducts as a reducing system. *J. Organomet. Chem.* **2011**, *696*, 1803–1808. [[CrossRef](#)]
42. Chen, H.; Yu, Z.J.; Xu, D.D.; Li, Y.; Wang, M.M.; Xia, L.M.; Shu-Ping, L. In-Situ Formed Amorphous Co Nanoparticles for Efficiently Catalytic Hydrogen Production from the Methanolysis of Ammonia Borane. *Chin. J. Inorg. Chem.* **2019**, *35*, 141–148.
43. Yu, C.; Fu, J.J.; Muzzio, M.; Shen, T.L.; Su, D.; Zhu, J.J.; Sun, S.H. CuNi nanoparticles assembled on graphene for catalytic methanolysis of ammonia borane and hydrogenation of nitro/nitrile compounds. *Chem. Mater.* **2017**, *29*, 1413–1418. [[CrossRef](#)]
44. Özhava, D.; Kılıçaslan, N.Z.; Özkar, S. PVP-stabilized nickel (0) nanoparticles as catalyst in hydrogen generation from the methanolysis of hydrazine borane or ammonia borane. *Appl. Catal. B Environ.* **2015**, *162*, 573–582. [[CrossRef](#)]
45. Heldebrant, D.J.; Karkamkar, A.; Hess, N.J.; Bowden, M.; Rassat, S.; Zheng, F.; Kenneth, R.; Autrey, T. The effects of chemical additives on the induction phase in solid-state thermal decomposition of ammonia borane. *Chem. Mater.* **2008**, *20*, 5332–5336. [[CrossRef](#)]
46. Rueda, M.; Sanz-Moral, L.M.; Segovia, J.J.; Martín, Á. Improvement of the kinetics of hydrogen release from ammonia borane confined in silica aerogel. *Microporous Mesoporous Mater.* **2017**, *237*, 189–200. [[CrossRef](#)]
47. Zhang, X.Y.; Kam, L.; Trerise, R.; Williams, T.J. Ruthenium-catalyzed ammonia borane dehydrogenation: Mechanism and utility. *Acc. Chem. Res.* **2017**, *50*, 86–95. [[CrossRef](#)]
48. Gil-San-Millan, R.; Grau-Atiienza, A.; Johnson, D.T.; Rico-Francés, S.; Serrano, E.; Linares, N.; Garcia-Martinez, J. Improving hydrogen production from the hydrolysis of ammonia borane by using multifunctional catalysts. *Int. J. Hydrog. Energy* **2018**, *43*, 17100–17111. [[CrossRef](#)]
49. Du, X.Q.; Yang, C.L.; Zeng, X.; Wu, T.; Zhou, Y.H.; Cai, P.; Cheng, G.Z.; Luo, W. Amorphous NiP supported on rGO for superior hydrogen generation from hydrolysis of ammonia borane. *Int. J. Hydrog. Energy* **2017**, *42*, 14181–14187. [[CrossRef](#)]

50. Zhang, M.Y.; Xiao, X.; Wu, Y.; An, Y.; Xu, L.X.; Wan, C. Hydrogen Production from Ammonia Borane over PtNi Alloy Nanoparticles Immobilized on Graphite Carbon Nitride. *Catalysts* **2019**, *9*, 1009. [[CrossRef](#)]
51. Kim, S.K.; Han, W.S.; Kim, T.J.; Kim, T.Y.; Nam, S.W.; Mitoraj, M.; Piekos, L.; Michalak, A.; Hwang, S.J.; Kang, S.O. Palladium catalysts for dehydrogenation of ammonia borane with preferential B–H activation. *J. Am. Chem. Soc.* **2010**, *132*, 9954–9955. [[CrossRef](#)] [[PubMed](#)]
52. Yousef, A.; Brooks, R.M.; El-Halwany, M.M.; Abutaleb, A.; El-Newehy, M.H.; Al-Deyab, S.S.; Kim, H.Y. Electrospun CoCr<sub>7</sub>C<sub>3</sub>-supported C nanofibers: Effective, durable, and chemically stable catalyst for H<sub>2</sub> gas generation from ammonia borane. *Mol. Catal.* **2017**, *434*, 32–38. [[CrossRef](#)]
53. Figen, A.K.; Filiz, B.C. Polymeric and metal oxide structured nanofibrous composites fabricated by electrospinning as highly efficient hydrogen evolution catalyst. *J. Colloid Interface Sci.* **2019**, *533*, 82–94. [[CrossRef](#)] [[PubMed](#)]
54. Alpaydin, C.Y.; Gülbay, S.K.; Colpan, C.O. A review on the catalysts used for hydrogen production from ammonia borane. *Int. J. Hydrog. Energy* **2020**, *45*, 3414–3434. [[CrossRef](#)]
55. Brockman, A.; Zheng, Y.; Gore, J. A study of catalytic hydrolysis of concentrated ammonia borane solutions. *Int. J. Hydrog. Energy* **2010**, *35*, 7350–7356. [[CrossRef](#)]
56. Manna, J.; Akbayrak, S.; Özkar, S. Palladium (0) nanoparticles supported on polydopamine coated CoFe<sub>2</sub>O<sub>4</sub> as highly active, magnetically isolable and reusable catalyst for hydrogen generation from the hydrolysis of ammonia borane. *Appl. Catal. B Environ.* **2017**, *208*, 104–115. [[CrossRef](#)]
57. Xu, L.X.; Yao, F.; Luo, J.L.; Wan, C.; Ye, M.F.; Cui, P.; An, Y. Facile synthesis of amine-functionalized SBA-15-supported bimetallic Au–Pd nanoparticles as an efficient catalyst for hydrogen generation from formic acid. *RSC Adv.* **2017**, *7*, 4746–4752. [[CrossRef](#)]
58. Xu, Q.; Chandra, M. A portable hydrogen generation system: Catalytic hydrolysis of ammonia–borane. *J. Alloy. Compd.* **2007**, *446*, 729–732. [[CrossRef](#)]
59. Chandra, M.; Xu, Q. Room temperature hydrogen generation from aqueous ammonia-borane using noble metal nano-clusters as highly active catalysts. *J. Power Sources* **2007**, *168*, 135–142. [[CrossRef](#)]
60. Chen, W.Y.; Ji, J.; Duan, X.Z.; Qian, G.; Li, P.; Zhou, X.G.; Chen, D.; Yuan, W.K. Unique reactivity in Pt/CNT catalyzed hydrolytic dehydrogenation of ammonia borane. *Chem. Commun.* **2014**, *50*, 2142–2144. [[CrossRef](#)] [[PubMed](#)]
61. Durap, F.; Zahmakıran, M.; Özkar, S. Water soluble laurate-stabilized ruthenium (0) nanoclusters catalyst for hydrogen generation from the hydrolysis of ammonia-borane: High activity and long lifetime. *Int. J. Hydrog. Energy* **2009**, *34*, 7223–7230. [[CrossRef](#)]
62. Cao, N.; Luo, W.; Cheng, G.Z. One-step synthesis of graphene supported Ru nanoparticles as efficient catalysts for hydrolytic dehydrogenation of ammonia borane. *Int. J. Hydrog. Energy* **2013**, *38*, 11964–11972. [[CrossRef](#)]
63. Liang, H.Y.; Chen, G.Z.; Desinan, S.; Rosei, R.; Rosei, F.; Ma, D.L. In situ facile synthesis of ruthenium nanocluster catalyst supported on carbon black for hydrogen generation from the hydrolysis of ammonia-borane. *Int. J. Hydrog. Energy* **2012**, *37*, 17921–17927. [[CrossRef](#)]
64. Du, C.; Ao, Q.; Cao, N.; Yang, L.; Luo, W.; Cheng, G.Z. Facile synthesis of monodisperse ruthenium nanoparticles supported on graphene for hydrogen generation from hydrolysis of ammonia borane. *Int. J. Hydrog. Energy* **2015**, *40*, 6180–6187. [[CrossRef](#)]
65. Wen, L.; Su, J.; Wu, X.J.; Cai, P.; Luo, W.; Cheng, G.Z. Ruthenium supported on MIL-96: An efficient catalyst for hydrolytic dehydrogenation of ammonia borane for chemical hydrogen storage. *Int. J. Hydrog. Energy* **2014**, *39*, 17129–17135. [[CrossRef](#)]
66. Yang, K.Z.; Zhou, L.Q.; Yu, G.F.; Xiong, X.; Ye, M.L.; Li, Y.; Lu, D.; Pan, Y.X.; Chen, M.H.; Zhang, L.; et al. Ru nanoparticles supported on MIL-53 (Cr, Al) as efficient catalysts for hydrogen generation from hydrolysis of ammonia borane. *Int. J. Hydrog. Energy* **2016**, *41*, 6300–6309. [[CrossRef](#)]
67. Fan, G.Y.; Liu, Q.Q.; Tang, D.M.; Li, X.J.; Bi, J.; Gao, D.J. Nanodiamond supported Ru nanoparticles as an effective catalyst for hydrogen evolution from hydrolysis of ammonia borane. *Int. J. Hydrog. Energy* **2016**, *41*, 1542–1549. [[CrossRef](#)]
68. Wu, Z.J.; Duan, Y.L.; Ge, S.H.; Yip, A.C.; Yang, F.; Li, Y.F.; Dou, T. Promoting hydrolysis of ammonia borane over multiwalled carbon nanotube-supported Ru catalysts via hydrogen spillover. *Catal. Commun.* **2017**, *91*, 10–15. [[CrossRef](#)]

69. Yao, Q.L.; Shi, W.M.; Feng, G.; Lu, Z.H.; Zhang, X.L.; Tao, D.J.; Kong, D.J.; Chen, X.S. Ultrafine Ru nanoparticles embedded in SiO<sub>2</sub> nanospheres: Highly efficient catalysts for hydrolytic dehydrogenation of ammonia borane. *J. Power Sources* **2014**, *257*, 293–299. [[CrossRef](#)]
70. Akbayrak, S.; Tonbul, Y.; Özkaz, S. Ceria supported rhodium nanoparticles: Superb catalytic activity in hydrogen generation from the hydrolysis of ammonia borane. *Appl. Catal. B Environ.* **2016**, *198*, 162–170. [[CrossRef](#)]
71. Özhava, D.; Özkaz, S. Rhodium (0) nanoparticles supported on nanosilica: Highly active and long lived catalyst in hydrogen generation from the methanolysis of ammonia borane. *Appl. Catal. B Environ.* **2016**, *181*, 716–726. [[CrossRef](#)]
72. Roy, S.; Pachfule, P.; Xu, Q. High Catalytic Performance of MIL-101-Immobilized NiRu Alloy Nanoparticles towards the Hydrolytic Dehydrogenation of Ammonia Borane. *Eur. J. Inorg. Chem.* **2016**, *2016*, 4353–4357. [[CrossRef](#)]
73. Yao, Q.L.; Lu, Z.H.; Wang, Y.Q.; Chen, X.S.; Feng, G. Synergetic catalysis of non-noble bimetallic Cu–Co nanoparticles embedded in SiO<sub>2</sub> nanospheres in hydrolytic dehydrogenation of ammonia borane. *J. Phys. Chem. C* **2015**, *119*, 14167–14174. [[CrossRef](#)]
74. Fernandes, R.; Patel, N.; Edla, R.; Bazzanella, N.; Kothari, D.C.; Miotello, A. Ruthenium nanoparticles supported over carbon thin film catalyst synthesized by pulsed laser deposition for hydrogen production from ammonia borane. *Appl. Catal. A Gen.* **2015**, *495*, 23–29. [[CrossRef](#)]
75. Park, J.W.; Lai, S.W.; Cho, S.O. Catalytic hydrogen generation from hydrolysis of ammonia borane using octahedral Au@Pt nanoparticles. *Int. J. Hydrog. Energy* **2015**, *40*, 16316–16322. [[CrossRef](#)]
76. Shen, J.F.; Yang, L.; Hu, K.; Luo, W.; Cheng, G.Z. Rh nanoparticles supported on graphene as efficient catalyst for hydrolytic dehydrogenation of amine boranes for chemical hydrogen storage. *Int. J. Hydrog. Energy* **2015**, *40*, 1062–1070. [[CrossRef](#)]
77. Xia, B.Q.; Liu, C.; Wu, H.; Luo, W.; Cheng, G.Z. Hydrolytic dehydrogenation of ammonia borane catalyzed by metal-organic framework supported bimetallic RhNi nanoparticles. *Int. J. Hydrog. Energy* **2015**, *40*, 16391–16397. [[CrossRef](#)]
78. Shang, N.Z.; Feng, C.; Gao, S.T.; Wang, C. Ag/Pd nanoparticles supported on amine-functionalized metal-organic framework for catalytic hydrolysis of ammonia borane. *Int. J. Hydrog. Energy* **2016**, *41*, 944–950. [[CrossRef](#)]
79. Rakap, M. The highest catalytic activity in the hydrolysis of ammonia borane by poly (N-vinyl-2-pyrrolidone)-protected palladium–rhodium nanoparticles for hydrogen generation. *Appl. Catal. B Environ.* **2015**, *163*, 129–134. [[CrossRef](#)]
80. Sullivan, J.A.; Herron, R.; Phillips, A.D. Towards an understanding of the beneficial effect of mesoporous materials on the dehydrogenation characteristics of NH<sub>3</sub>BH<sub>3</sub>. *Appl. Catal. B Environ.* **2017**, *201*, 182–188. [[CrossRef](#)]
81. Zhang, T.R.; Yang, X.J.; Yang, S.Q.; Li, D.X.; Cheng, F.Y.; Tao, Z.L.; Chen, J. Silica hollow nanospheres as new nanoscaffold materials to enhance hydrogen releasing from ammonia borane. *Phys. Chem. Chem. Phys.* **2011**, *13*, 18592–18599. [[CrossRef](#)] [[PubMed](#)]
82. Xu, L.X.; Liu, N.; Hong, B.; Cui, P.; Cheng, D.G.; Chen, F.Q.; An, Y.; Wan, C. Nickel–platinum nanoparticles immobilized on graphitic carbon nitride as highly efficient catalyst for hydrogen release from hydrous hydrazine. *RSC Adv.* **2016**, *6*, 31687–31691. [[CrossRef](#)]
83. Kuhn, J.N.; Huang, W.Y.; Tsung, C.K.; Zhang, Y.W.; Somorjai, G.A. Structure sensitivity of carbon–nitrogen ring opening: Impact of platinum particle size from below 1 to 5 nm upon pyrrole hydrogenation product selectivity over monodisperse platinum nanoparticles loaded onto mesoporous silica. *J. Am. Chem. Soc.* **2008**, *130*, 14026–14027. [[CrossRef](#)] [[PubMed](#)]
84. Tsung, C.K.; Kuhn, J.N.; Huang, W.Y.; Aliaga, C.; Hung, L.I.; Somorjai, G.A.; Yang, P. Sub-10 nm platinum nanocrystals with size and shape control: Catalytic study for ethylene and pyrrole hydrogenation. *J. Am. Chem. Soc.* **2009**, *131*, 5816–5822. [[CrossRef](#)]
85. Arenz, M.; Mayrhofer, K.J.; Stamenkovic, V.; Blizanac, B.B.; Tomoyuki, T.; Ross, P.N.; Markovic, N.M. The effect of the particle size on the kinetics of CO electrooxidation on high surface area Pt catalysts. *J. Am. Chem. Soc.* **2005**, *127*, 6819–6829. [[CrossRef](#)] [[PubMed](#)]

86. Allian, A.D.; Takanahe, K.; Furdala, K.L.; Hao, X.H.; Truex, T.J.; Cai, J.; Buda, C.; Neurock, M.; Iglesia, E. Chemisorption of CO and mechanism of CO oxidation on supported platinum nanoclusters. *J. Am. Chem. Soc.* **2011**, *133*, 4498–4517. [[CrossRef](#)]
87. Chin, Y.H.; Buda, C.; Neurock, M.; Iglesia, E. Reactivity of chemisorbed oxygen atoms and their catalytic consequences during CH<sub>4</sub>-O<sub>2</sub> catalysis on supported Pt clusters. *J. Am. Chem. Soc.* **2011**, *133*, 15958–15978. [[CrossRef](#)] [[PubMed](#)]
88. Yao, K.S.; Zhao, C.C.; Wang, N.; Li, T.J.; Lu, W.W.; Wang, J.J. An aqueous synthesis of porous PtPd nanoparticles with reversed bimetallic structures for highly efficient hydrogen generation from ammonia borane hydrolysis. *Nanoscale* **2020**, *12*, 638–647. [[CrossRef](#)]
89. Zhou, M.; Wang, H.L.; Vara, M.; Hood, Z.D.; Luo, M.; Yang, T.H.; Bao, S.X.; Chi, M.F.; Xiao, P.; Zhang, Y.H.; et al. Quantitative analysis of the reduction kinetics responsible for the one-pot synthesis of Pd–Pt bimetallic nanocrystals with different structures. *J. Am. Chem. Soc.* **2016**, *138*, 12263–12270. [[CrossRef](#)]
90. Käß, M.; Friedrich, A.; Drees, M.; Schneider, S. Ruthenium complexes with cooperative PNP ligands: Bifunctional catalysts for the dehydrogenation of ammonia–borane. *Angew. Chem. Int. Ed.* **2009**, *48*, 905–907. [[CrossRef](#)]
91. Wen, L.; Zheng, Z.; Luo, W.; Cai, P.; Cheng, G.Z. Ruthenium deposited on MCM-41 as efficient catalyst for hydrolytic dehydrogenation of ammonia borane and methylamine borane. *Chin. Chem. Lett.* **2015**, *26*, 1345–1350. [[CrossRef](#)]
92. Xu, C.X.; Su, J.X.; Xu, X.H.; Liu, P.P.; Zhao, H.J.; Tian, F.; Ding, Y. Low temperature CO oxidation over unsupported nanoporous gold. *J. Am. Chem. Soc.* **2007**, *129*, 42–43. [[CrossRef](#)] [[PubMed](#)]
93. Yu, L.B.; Shi, Y.Y.; Zhao, Z.; Yin, H.B.; Wei, Y.C.; Liu, J.; Kang, W.B.; Jiang, T.S.; Wang, A.L. Ultrasmall silver nanoparticles supported on silica and their catalytic performances for carbon monoxide oxidation. *Catal. Commun.* **2011**, *12*, 616–620. [[CrossRef](#)]
94. Huang, L.; Zou, J.S.; Ye, J.Y.; Zhou, Z.Y.; Lin, Z.; Kang, X.W.; Jain, P.; Chen, S.W. Synergy between Plasmonic and Electrocatalytic Activation of Methanol Oxidation on Palladium–Silver Alloy Nanotubes. *Angew. Chem.* **2019**, *131*, 8886–8890. [[CrossRef](#)]
95. Wu, Y.; Jiao, L.; Xu, W.Q.; Gu, W.L.; Zhu, C.Z.; Du, D.; Lin, Y.H. Polydopamine-Capped Bimetallic AuPt Hydrogels Enable Robust Biosensor for Organophosphorus Pesticide Detection. *Small* **2019**, *15*, 1900632. [[CrossRef](#)]
96. Lv, H.; Sun, L.Z.; Zou, L.; Xu, D.D.; Yao, H.Q.; Liu, B. Size-dependent synthesis and catalytic activities of trimetallic PdAgCu mesoporous nanospheres in ethanol electrooxidation. *Chem. Sci.* **2019**, *10*, 1986–1993. [[CrossRef](#)]
97. Abo-Hamed, E.; Pennycook, T.; Vaynzof, Y.; Toprakcioglu, C.; Koutsioubas, A.; Scherman, O.A. Highly active metastable ruthenium nanoparticles for hydrogen production through the catalytic hydrolysis of ammonia borane. *Small* **2014**, *10*, 3145–3152. [[CrossRef](#)]
98. Wan, C.; An, Y.; Chen, F.Q.; Cheng, D.G.; Wu, F.Y.; Xu, G.H. Kinetics of N-ethylcarbazole hydrogenation over a supported Ru catalyst for hydrogen storage. *Int. J. Hydrogen Energy* **2013**, *38*, 7065–7069. [[CrossRef](#)]
99. Du, J.; Cheng, F.Y.; Si, M.; Liang, J.; Tao, Z.L.; Chen, J. Nanoporous Ni-based catalysts for hydrogen generation from hydrolysis of ammonia borane. *Int. J. Hydrog. Energy* **2013**, *38*, 5768–5774. [[CrossRef](#)]
100. Li, Y.; Dai, Y.; Tian, X.K. Controlled synthesis of monodisperse Pd<sub>x</sub>Sn<sub>100-x</sub> nanoparticles and their catalytic activity for hydrogen generation from the hydrolysis of ammonia-borane. *Int. J. Hydrog. Energy* **2015**, *40*, 9235–9243.
101. Güngörmez, K.; Metin, Ö. Composition-controlled catalysis of reduced graphene oxide supported CuPd alloy nanoparticles in the hydrolytic dehydrogenation of ammonia borane. *Appl. Catal. A Gen.* **2015**, *494*, 22–28. [[CrossRef](#)]
102. Zhang, J.; Dong, Y.; Liu, Q.X.; Zhou, M.; Mi, G.; Du, X.G. Hierarchically alloyed Pd–Cu microarchitecture with tunable shapes: Morphological engineering, and catalysis for hydrogen evolution reaction of ammonia borane. *Int. J. Hydrog. Energy* **2019**, *44*, 30226–30236. [[CrossRef](#)]
103. Deka, J.R.; Saikia, D.; Chen, P.H.; Chen, K.T.; Kao, H.M.; Yang, Y.C. Palladium nanoparticles encapsulated in carboxylic acid functionalized periodic mesoporous organosilicas as efficient and reusable heterogeneous catalysts for hydrogen generation from ammonia borane. *Materials Research Bulletin* **2020**, *125*, 110786. [[CrossRef](#)]

104. Wang, K.; Zhang, J.G.; Man, T.T.; Wu, M.; Chen, C.C. Recent process and development of metal aminoborane. *Chem. Asian J.* **2013**, *8*, 1076–1089. [[CrossRef](#)] [[PubMed](#)]
105. Zhou, X.; Meng, X.F.; Wang, J.M.; Shang, N.Z.; Feng, T.; Gao, Z.Y.; Zhang, H.X.; Ding, X.L.; Gao, S.T.; Feng, C.; et al. Boron nitride supported NiCoP nanoparticles as noble metal-free catalyst for highly efficient hydrogen generation from ammonia borane. *Int. J. Hydrog. Energy* **2019**, *44*, 4764–4770. [[CrossRef](#)]
106. Singh, A.K.; Xu, Q. Synergistic catalysis over bimetallic alloy nanoparticles. *ChemCatChem* **2013**, *5*, 652–676. [[CrossRef](#)]
107. Yang, L.; Su, J.; Meng, X.Y.; Luo, W.; Cheng, G.Z. In situ synthesis of graphene supported Ag@CoNi core-shell nanoparticles as highly efficient catalysts for hydrogen generation from hydrolysis of ammonia borane and methylamine borane. *J. Mater. Chem. A* **2013**, *1*, 10016–10023. [[CrossRef](#)]
108. El-Sayed, M.A. Some interesting properties of metals confined in time and nanometer space of different shapes. *Acc. Chem. Res.* **2001**, *34*, 257–264. [[CrossRef](#)]
109. Chen, H.M.; Liu, R.S. Architecture of metallic nanostructures: Synthesis strategy and specific applications. *J. Phys. Chem. C* **2011**, *115*, 3513–3527. [[CrossRef](#)]
110. Chen, S.W.; Yang, Y.Y. Magneto-electrochemistry of gold nanoparticle quantized capacitance charging. *J. Am. Chem. Soc.* **2002**, *124*, 5280–5281. [[CrossRef](#)]
111. Yang, X.J.; Cheng, F.Y.; Liang, J.; Tao, Z.L.; Chen, J. Pt<sub>x</sub>Ni<sub>1-x</sub> nanoparticles as catalysts for hydrogen generation from hydrolysis of ammonia borane. *Int. J. Hydrog. Energy* **2009**, *34*, 8785–8791. [[CrossRef](#)]
112. Gao, M.Y.; Yang, W.W.; Yu, Y.S. Monodisperse PtCu alloy nanoparticles as highly efficient catalysts for the hydrolytic dehydrogenation of ammonia borane. *Int. J. Hydrog. Energy* **2018**, *43*, 14293–14300. [[CrossRef](#)]
113. Chen, W.Y.; Fu, W.Z.; Qian, G.; Zhang, B.S.; Chen, D.; Duan, X.Z.; Zhou, X.G. Synergistic Pt-WO<sub>3</sub> Dual Active Sites to Boost Hydrogen Production from Ammonia Borane. *Iscience* **2020**, *23*, 100922. [[CrossRef](#)]
114. Akbayrak, S.; Özkar, S. Ammonia borane as hydrogen storage materials. *Int. J. Hydrog. Energy* **2018**, *43*, 18592–18606. [[CrossRef](#)]
115. Zahmakiran, M.; Özkar, S. Transition metal nanoparticles in catalysis for the hydrogen generation from the hydrolysis of ammonia-borane. *Top. Catal.* **2013**, *56*, 1171–1183. [[CrossRef](#)]
116. Özkar, S.; Finke, R.G. Nanocluster formation and stabilization fundamental studies: Ranking commonly employed anionic stabilizers via the development, then application, of five comparative criteria. *J. Am. Chem. Soc.* **2002**, *124*, 5796–5810. [[CrossRef](#)]
117. Shylesh, S.; Schuenemann, V.; Thiel, W.R. Magnetically separable nanocatalysts: Bridges between homogeneous and heterogeneous catalysis. *Angew. Chem. Int. Ed.* **2010**, *49*, 3428–3459. [[CrossRef](#)]
118. Baig, R.N.; Varma, R.S. Magnetically retrievable catalysts for organic synthesis. *Chem. Commun.* **2013**, *49*, 752–770. [[CrossRef](#)]
119. Wang, D.; Astruc, D. Fast-growing field of magnetically recyclable nanocatalysts. *Chem. Rev.* **2014**, *114*, 6949–6985. [[CrossRef](#)]
120. Akbayrak, S.; Çakmak, G.; Öztürk, T.; Özkar, S. Rhodium (0), Ruthenium (0) and Palladium (0) nanoparticles supported on carbon-coated iron: Magnetically isolable and reusable catalysts for hydrolytic dehydrogenation of ammonia borane. *Int. J. Hydrog. Energy* **2020**. [[CrossRef](#)]
121. Zhou, Q.X.; Yang, H.X.; Xu, C.X. Nanoporous Ru as highly efficient catalyst for hydrolysis of ammonia borane. *Int. J. Hydrog. Energy* **2016**, *41*, 12714–12721. [[CrossRef](#)]
122. Wei, Z.H.; Liu, Y.; Peng, Z.K.; Song, H.Q.; Liu, Z.Y.; Liu, B.Z.; Li, B.Z.; Yang, B.; Lu, S.Y. Cobalt-ruthenium nanoalloys parceled in porous nitrogen-doped graphene as highly efficient difunctional catalysts for hydrogen evolution reaction and hydrolysis of ammonia borane. *ACS Sustain. Chem. Eng.* **2019**, *7*, 7014–7023. [[CrossRef](#)]
123. Guo, L.T.; Cai, Y.Y.; Ge, J.M.; Zhang, Y.N.; Gong, L.H.; Li, X.H.; Wang, K.X.; Ren, Q.Z.; Su, J.; Chen, J.S. Multifunctional Au-Co@CN nanocatalyst for highly efficient hydrolysis of ammonia borane. *ACS Catal.* **2015**, *5*, 388–392. [[CrossRef](#)]
124. Liu, Y.; Wang, Q.H.; Wu, L.L.; Long, Y.; Li, J.; Song, S.Y.; Zhang, H.J. Tunable bimetallic Au-Pd@CeO<sub>2</sub> for semihydrogenation of phenylacetylene by ammonia borane. *Nanoscale* **2019**, *11*, 12932–12937. [[CrossRef](#)] [[PubMed](#)]
125. Wang, Q.; Fu, F.Y.; Yang, S.; Martinez Moro, M.; Ramirez, M.D.L.A.; Moya, S.; Moya, S.; Salmon, L.; Ruiz, J.; Astruc, D. Dramatic synergy in CoPt nanocatalysts stabilized by “Click” dendrimers for evolution of hydrogen from hydrolysis of ammonia borane. *ACS Catal.* **2018**, *9*, 1110–1119. [[CrossRef](#)]

126. Zhou, Q.X.; Qi, L.; Yang, H.X.; Xu, C.X. Hierarchical nanoporous platinum–copper alloy nanoflowers as highly active catalysts for the hydrolytic dehydrogenation of ammonia borane. *J. Colloid Interface Sci.* **2018**, *513*, 258–265. [[CrossRef](#)]
127. Yang, X.; Li, Q.L.; Li, L.L.; Lin, J.; Yang, X.J.; Yu, C.; Liu, Z.Y.; Fang, Y.; Huang, Y.F.; Tang, C.C. CuCo binary metal nanoparticles supported on boron nitride nanofibers as highly efficient catalysts for hydrogen generation from hydrolysis of ammonia borane. *J. Power Sources* **2019**, *431*, 135–143. [[CrossRef](#)]
128. Haruta, M.; Daté, M. Advances in the catalysis of Au nanoparticles. *Appl. Catal. A Gen.* **2001**, *222*, 427–437. [[CrossRef](#)]
129. Haruta, M.; Yamada, N.; Kobayashi, T.; Iijima, S. Gold catalysts prepared by coprecipitation for low-temperature oxidation of hydrogen and of carbon monoxide. *J. Catal.* **1989**, *115*, 301–309. [[CrossRef](#)]
130. Jiang, H.L.; Umegaki, T.; Akita, T.; Zhang, X.B.; Haruta, M.; Xu, Q. Bimetallic Au–Ni nanoparticles embedded in SiO<sub>2</sub> nanospheres: Synergetic catalysis in hydrolytic dehydrogenation of ammonia borane. *Chem. A Eur. J.* **2010**, *16*, 3132–3137. [[CrossRef](#)]
131. Rej, S.; Hsia, C.F.; Chen, T.Y.; Lin, F.C.; Huang, J.S.; Huang, M.H. Facet-Dependent and Light-Assisted Efficient Hydrogen Evolution from Ammonia Borane Using Gold–Palladium Core-Shell Nanocatalysts. *Angew. Chem. Int. Ed.* **2016**, *55*, 7222–7226. [[CrossRef](#)] [[PubMed](#)]
132. Lv, H.F.; Xi, Z.; Chen, Z.Z.; Guo, S.J.; Yu, Y.S.; Zhu, W.L.; Li, Q.; Zhang, X.; Pan, M.; Lu, G.; et al. A new core/shell NiAu/Au nanoparticle catalyst with Pt-like activity for hydrogen evolution reaction. *J. Am. Chem. Soc.* **2015**, *137*, 5859–5862. [[CrossRef](#)] [[PubMed](#)]
133. Gong, K.P.; Su, D.; Adzic, R.R. Platinum-monolayer shell on AuNi<sub>0.5</sub>Fe nanoparticle core electrocatalyst with high activity and stability for the oxygen reduction reaction. *J. Am. Chem. Soc.* **2010**, *132*, 14364–14366. [[CrossRef](#)] [[PubMed](#)]
134. Kang, J.X.; Chen, T.W.; Zhang, D.F.; Guo, L. PtNiAu trimetallic nanoalloys enabled by a digestive-assisted process as highly efficient catalyst for hydrogen generation. *Nano Energy* **2016**, *23*, 145–152. [[CrossRef](#)]
135. Yamauchi, Y.; Tonegawa, A.; Komatsu, M.; Wang, H.J.; Wang, L.; Nemoto, Y.; Suzuki, N.; Kuroda, K. Electrochemical synthesis of mesoporous Pt–Au binary alloys with tunable compositions for enhancement of electrochemical performance. *J. Am. Chem. Soc.* **2012**, *134*, 5100–5109. [[CrossRef](#)]
136. Fu, L.L.; Zhang, D.F.; Yang, Z.; Chen, T.W.; Zhai, J. PtAuCo Trimetallic Nanoalloys as Highly Efficient Catalysts toward Dehydrogenation of Ammonia Borane. *ACS Sustain. Chem. Eng.* **2020**, *8*, 3734–3742. [[CrossRef](#)]
137. Shui, J.L.; Chen, C.; Li, J.C. Evolution of nanoporous Pt–Fe alloy nanowires by dealloying and their catalytic property for oxygen reduction reaction. *Adv. Funct. Mater.* **2011**, *21*, 3357–3362. [[CrossRef](#)]
138. Cui, C.H.; Gan, L.; Li, H.H.; Yu, S.H.; Heggen, M.; Strasser, P. Octahedral PtNi nanoparticle catalysts: Exceptional oxygen reduction activity by tuning the alloy particle surface composition. *Nano Lett.* **2012**, *12*, 5885–5889. [[CrossRef](#)]
139. Xia, B.Y.; Wu, H.B.; Li, N.; Yan, Y.; Lou, X.W.; Wang, X. One-pot synthesis of Pt–Co alloy nanowire assemblies with tunable composition and enhanced electrocatalytic properties. *Angew. Chem. Int. Ed.* **2015**, *54*, 3797–3801. [[CrossRef](#)]
140. Zhang, Z.C.; Luo, Z.M.; Chen, B.; Wei, C.; Zhao, J.; Chen, J.Z.; Zhang, X.; Lai, Z.C.; Fan, Z.X.; Tan, C.L.; et al. One-pot synthesis of highly anisotropic five-fold-twinned PtCu nanoframes used as a bifunctional electrocatalyst for oxygen reduction and methanol oxidation. *Adv. Mater.* **2016**, *28*, 8712–8717. [[CrossRef](#)]
141. Bu, L.Z.; Shao, Q.; Bin, E.; Guo, J.; Yao, J.L.; Huang, X.Q. PtPb/PtNi intermetallic core/atomic layer shell octahedra for efficient oxygen reduction electrocatalysis. *J. Am. Chem. Soc.* **2017**, *139*, 9576–9582. [[CrossRef](#)] [[PubMed](#)]
142. Meng, C.; Ling, T.; Ma, T.Y.; Wang, H.; Hu, Z.P.; Zhou, Y.; Mao, J.; Du, X.W.; Jaroniec, M.; Qiao, S.Z. Atomically and electronically coupled Pt and CoO hybrid nanocatalysts for enhanced electrocatalytic performance. *Adv. Mater.* **2017**, *29*, 1604607. [[CrossRef](#)] [[PubMed](#)]
143. Xu, C.L.; Hu, M.; Wang, Q.; Fan, G.Y.; Wang, Y.; Zhang, Y.; Gao, D.J.; Bi, J. Hyper-cross-linked polymer supported rhodium: An effective catalyst for hydrogen evolution from ammonia borane. *Dalton Trans.* **2018**, *47*, 2561–2567. [[CrossRef](#)]
144. Zhong, F.Y.; Wang, Q.; Xu, C.L.; Yang, Y.C.; Wang, Y.; Zhang, Y.; Gao, D.J.; Bi, J.; Fan, G. Ultrafine and highly dispersed Ru nanoparticles supported on nitrogen-doped carbon nanosheets: Efficient catalysts for ammonia borane hydrolysis. *Appl. Surf. Sci.* **2018**, *455*, 326–332. [[CrossRef](#)]

145. Metin, Ö.; Kayhan, E.; Özkar, S.; Schneider, J.J. Palladium nanoparticles supported on chemically derived graphene: An efficient and reusable catalyst for the dehydrogenation of ammonia borane. *Int. J. Hydrog. Energy* **2012**, *37*, 8161–8169. [[CrossRef](#)]
146. Lu, R.; Xu, C.L.; Wang, Q.; Wang, Y.; Zhang, Y.; Gao, D.J.; Bi, J.; Fan, G.Y. Ruthenium nanoclusters distributed on phosphorus-doped carbon derived from hypercrosslinked polymer networks for highly efficient hydrolysis of ammonia-borane. *Int. J. Hydrog. Energy* **2018**, *43*, 18253–18260. [[CrossRef](#)]
147. Yao, Q.L.; Lu, Z.H.; Jia, Y.S.; Chen, X.S.; Liu, X. In situ facile synthesis of Rh nanoparticles supported on carbon nanotubes as highly active catalysts for H<sub>2</sub> generation from NH<sub>3</sub>BH<sub>3</sub> hydrolysis. *Int. J. Hydrog. Energy* **2015**, *40*, 2207–2215. [[CrossRef](#)]
148. Hu, Y.J.; Wang, Y.Q.; Lu, Z.H.; Chen, X.S.; Xiong, L.H. Core-shell nanospheres Pt@SiO<sub>2</sub> for catalytic hydrogen production. *Appl. Surf. Sci.* **2015**, *341*, 185–189. [[CrossRef](#)]
149. Tonbul, Y.; Akbayrak, S.; Özkar, S. Palladium (0) nanoparticles supported on ceria: Highly active and reusable catalyst in hydrogen generation from the hydrolysis of ammonia borane. *Int. J. Hydrog. Energy* **2016**, *41*, 11154–11162. [[CrossRef](#)]
150. Akbayrak, S.; Tanyıldızı, S.; Morkan, İ.; Özkar, S. Ruthenium (0) nanoparticles supported on nanotitania as highly active and reusable catalyst in hydrogen generation from the hydrolysis of ammonia borane. *Int. J. Hydrog. Energy* **2014**, *39*, 9628–9637. [[CrossRef](#)]
151. Garaj, S.; Hubbard, W.; Reina, A.; Kong, J.; Branton, D.; Golovchenko, J.A. Graphene as a subnanometre trans-electrode membrane. *Nature* **2010**, *467*, 190–193. [[CrossRef](#)] [[PubMed](#)]
152. Choi, B.G.; Hong, J.; Park, Y.C.; Jung, D.H.; Hong, W.H.; Hammond, P.T.; Park, H. Innovative polymer nanocomposite electrolytes: Nanoscale manipulation of ion channels by functionalized graphenes. *ACS Nano* **2011**, *5*, 5167–5174. [[CrossRef](#)] [[PubMed](#)]
153. Novoselov, K.S.; Geim, A.K.; Morozov, S.V.; Jiang, D.; Zhang, Y.; Dubonos, S.V.; Grigorieva, I.V.; Firsov, A.A. Electric field effect in atomically thin carbon films. *Science* **2004**, *306*, 666–669. [[CrossRef](#)] [[PubMed](#)]
154. Guo, S.J.; Sun, S.H. FePt nanoparticles assembled on graphene as enhanced catalyst for oxygen reduction reaction. *J. Am. Chem. Soc.* **2012**, *134*, 2492–2495. [[CrossRef](#)]
155. Ke, D.D.; Wang, J.; Zhang, H.M.; Li, Y.; Zhang, L.; Zhao, X.; Han, S.M. Fabrication of Pt–Co NPs supported on nanoporous graphene as high-efficient catalyst for hydrolytic dehydrogenation of ammonia borane. *Int. J. Hydrog. Energy* **2017**, *42*, 26617–26625. [[CrossRef](#)]
156. Wang, S.; Zhang, D.; Ma, Y.Y.; Zhang, H.; Gao, J.; Nie, Y.T.; Sun, X.H. Aqueous solution synthesis of Pt–M (M = Fe, Co, Ni) bimetallic nanoparticles and their catalysis for the hydrolytic dehydrogenation of ammonia borane. *ACS Appl. Mater. Interfaces* **2014**, *6*, 12429–12435. [[CrossRef](#)]
157. Wang, J.M.; Ma, X.; Yang, W.R.; Sun, X.P.; Liu, J.Q. Self-supported Cu (OH)<sub>2</sub>@Co<sub>2</sub>CO<sub>3</sub>(OH)<sub>2</sub> core-shell nanowire array as a robust catalyst for ammonia-borane hydrolysis. *Nanotechnology* **2016**, *28*, 045606. [[CrossRef](#)] [[PubMed](#)]
158. Cheng, W.; Zhao, X.; Luo, W.X.; Zhang, Y.; Wang, Y.; Fan, G.Y. Bagasse-derived carbon supported Ru nanoparticles catalyst for efficient dehydrogenation of ammonia borane. *ChemNanoMat* **2020**, *6*, 1–10.
159. Men, Y.N.; Su, J.; Du, X.Q.; Liang, L.J.; Cheng, G.Z.; Luo, W. CoBP nanoparticles supported on three-dimensional nitrogen-doped graphene hydrogel and their superior catalysis for hydrogen generation from hydrolysis of ammonia borane. *J. Alloy. Compd.* **2018**, *735*, 1271–1276. [[CrossRef](#)]
160. Zhang, F.W.; Ma, C.; Zhang, Y.; Li, H.; Fu, D.Y.; Du, X.Q.; Zhang, X.M. N-doped mesoporous carbon embedded Co nanoparticles for highly efficient and stable H<sub>2</sub> generation from hydrolysis of ammonia borane. *J. Power Sources* **2018**, *399*, 89–97. [[CrossRef](#)]
161. Hou, C.C.; Li, Q.; Wang, C.J.; Peng, C.Y.; Chen, Q.Q.; Ye, H.F.; Fu, W.F.; Che, C.M.; López, N.; Chen, Y. Ternary Ni–Co–P nanoparticles as noble-metal-free catalysts to boost the hydrolytic dehydrogenation of ammonia-borane. *Energy Environ. Sci.* **2017**, *10*, 1770–1776. [[CrossRef](#)]
162. Panchakarla, L.S.; Subrahmanyam, K.S.; Saha, S.K.; Govindaraj, A.; Krishnamurthy, H.R.; Waghmare, U.V.; Rao, C.N.R. Synthesis, structure, and properties of boron-and nitrogen-doped graphene. *Adv. Mater.* **2009**, *21*, 4726–4730. [[CrossRef](#)]
163. Luo, W.L.; Zhao, X.; Cheng, W.; Zhang, Y.; Wang, Y.; Fan, G.F. A simple and straightforward strategy for synthesis of N, P co-doped porous carbon: An efficient support for Rh nanoparticles for dehydrogenation of ammonia borane and catalytic application. *Nanoscale Adv.* **2020**, *2*, 1685–1693. [[CrossRef](#)]

164. Hu, M.; Ming, M.X.; Xu, C.L.; Wang, Y.; Zhang, Y.; Gao, D.J.; Bi, J.; Fan, G.Y. Towards High-Efficiency Hydrogen Production through in situ Formation of Well-Dispersed Rhodium Nanoclusters. *ChemSusChem* **2018**, *11*, 3253–3258. [[CrossRef](#)]
165. Tonbul, Y.; Akbayrak, S.; Özkar, S. Group 4 oxides supported Rhodium (0) catalysts in hydrolytic dehydrogenation of ammonia borane. *Int. J. Hydrog. Energy* **2019**, *44*, 14164–14174. [[CrossRef](#)]
166. Chen, J.Q.; Hu, M.; Ming, M.; Xu, C.L.; Wang, Y.; Zhang, Y.; Wu, J.T.; Gao, G.J.; Bi, J.; Fan, G.Y. Carbon-supported small Rh nanoparticles prepared with sodium citrate: Toward high catalytic activity for hydrogen evolution from ammonia borane hydrolysis. *Int. J. Hydrog. Energy* **2018**, *43*, 2718–2725. [[CrossRef](#)]
167. Ai, W.; Zhou, W.W.; Du, Z.Z.; Chen, Y.; Sun, Z.P.; Wu, C.; Zou, C.J.; Li, C.M.; Huang, W.; Yu, T. Nitrogen and phosphorus codoped hierarchically porous carbon as an efficient sulfur host for Li-S batteries. *Energy Storage Mater.* **2017**, *6*, 112–118. [[CrossRef](#)]
168. Qin, Q.; Jang, H.; Chen, L.L.; Nam, G.; Liu, X.; Cho, J. Low loading of RhxP and RuP on N, P codoped carbon as two trifunctional electrocatalysts for the oxygen and hydrogen electrode reactions. *Adv. Energy Mater.* **2018**, *8*, 1801478. [[CrossRef](#)]
169. Liu, Y.; Yong, X.; Liu, Z.Y.; Chen, Z.M.; Kang, Z.H.; Lu, S.Y. Unified catalyst for efficient and stable hydrogen production by both the electrolysis of water and the hydrolysis of ammonia borane. *Adv. Sustain. Syst.* **2019**, *3*, 1800161. [[CrossRef](#)]
170. Song, H.Q.; Cheng, Y.J.; Li, B.J.; Fan, Y.P.; Liu, B.Z.; Tang, Z.Y.; Lu, S.Y. Carbon dots and RuP<sub>2</sub> nanohybrid as an efficient bifunctional catalyst for electrochemical hydrogen evolution reaction and hydrolysis of ammonia borane. *ACS Sustain. Chem. Eng.* **2020**, *8*, 3995–4002. [[CrossRef](#)]
171. Lv, Y.A.; Cui, Y.H.; Xiang, Y.Z.; Wang, J.G.; Li, X.N. Modulation of bonding between noble metal monomers and CNTs by B-, N-doping. *Comput. Mater. Sci.* **2010**, *48*, 621–625. [[CrossRef](#)]
172. Singh, P.; Samori, C.; Toma, F.M.; Bussy, C.; Nunes, A.; Al-Jamal, K.T.; Menard-Moyon, C.; Kostarelos, K.; Bianco, A. Polyamine functionalized carbon nanotubes: Synthesis, characterization, cytotoxicity and siRNA binding. *J. Mater. Chem.* **2011**, *21*, 4850–4860. [[CrossRef](#)]
173. Akbayrak, S.; Özkar, S. Ruthenium (0) nanoparticles supported on multiwalled carbon nanotube as highly active catalyst for hydrogen generation from ammonia-borane. *ACS Appl. Mater. Interfaces* **2012**, *4*, 6302–6310. [[CrossRef](#)]
174. Li, S.F.; Guo, Y.H.; Sun, W.W.; Sun, D.L.; Yu, X.B. Platinum nanoparticle functionalized CNTs as nanoscaffolds and catalysts to enhance the dehydrogenation of ammonia-borane. *J. Phys. Chem. C* **2010**, *114*, 21885–21890. [[CrossRef](#)]
175. Fu, W.; Han, C.; Li, D.; Chen, W.; Ji, J.; Qian, G.; Yuan, W.; Duan, X.; Zhou, X. Polyoxometalates-engineered hydrogen generation rate and durability of Pt/CNT catalysts from ammonia borane. *J. Energy Chem.* **2020**, *41*, 142–148. [[CrossRef](#)]
176. Lu, Z.H.; Jiang, H.L.; Yadav, M.; Aranishi, K.; Xu, Q. Synergistic catalysis of Au-Co@SiO<sub>2</sub> nanospheres in hydrolytic dehydrogenation of ammonia borane for chemical hydrogen storage. *J. Mater. Chem.* **2012**, *22*, 5065–5071. [[CrossRef](#)]
177. Metin, Ö.; Dinc, M.; Eren, Z.S.; Özkar, S. Silica embedded cobalt (0) nanoclusters: Efficient, stable and cost effective catalyst for hydrogen generation from the hydrolysis of ammonia borane. *Int. J. Hydrog. Energy* **2011**, *36*, 11528–11535. [[CrossRef](#)]
178. Umegaki, T.; Yan, J.M.; Zhang, X.B.; Shioyama, H.; Kuriyama, N.; Xu, Q. Co-SiO<sub>2</sub> nanosphere-catalyzed hydrolytic dehydrogenation of ammonia borane for chemical hydrogen storage. *J. Power Sources* **2010**, *195*, 8209–8214. [[CrossRef](#)]
179. Roy, B.; Manna, J.; Pal, U.; Hajari, A.; Bishnoi, A.; Sharma, P. An in situ study on the solid state decomposition of ammonia borane: Unmitigated by-product suppression by a naturally abundant layered clay mineral. *Inorg. Chem. Front.* **2018**, *5*, 301–309. [[CrossRef](#)]
180. Ye, W.Y.; Ge, Y.Z.; Gao, Z.M.; Lu, R.W.; Zhang, S.F. Enhanced catalytic activity and stability of Pt nanoparticles by surface coating of nanosized graphene oxide for hydrogen production from hydrolysis of ammonia-borane. *Sustain. Energy Fuels* **2017**, *1*, 2128–2133. [[CrossRef](#)]
181. Ciftci, A.; Eren, S.; Lighthart, D.M.; Hensen, E.J. Platinum-Rhenium Synergy on Reducible Oxide Supports in Aqueous-Phase Glycerol Reforming. *ChemCatChem* **2014**, *6*, 1260–1269. [[CrossRef](#)]

182. Badwal, S.P.S.; Fini, D.; Ciacchi, F.T.; Munnings, C.; Kimpton, J.A.; Drennan, J. Structural and microstructural stability of ceria–gadolinia electrolyte exposed to reducing environments of high temperature fuel cells. *J. Mater. Chem. A* **2013**, *1*, 10768–10782. [[CrossRef](#)]
183. Le Gal, A.; Abanades, S.; Bion, N.; Le Mercier, T.; Harléé, V. Reactivity of doped ceria-based mixed oxides for solar thermochemical hydrogen generation via two-step water-splitting cycles. *Energy Fuels* **2013**, *27*, 6068–6078. [[CrossRef](#)]
184. Hoare, J.P. *Standard Potentials in Aqueous Solution*; Marcel Dekker: New York, NY, USA, 1985; p. 49.
185. Lee, S.S.; Song, W.S.; Cho, M.J.; Puppala, H.L.; Nguyen, P.; Zhu, H.G.; Segatori, L.; Colvin, V.L. Antioxidant properties of cerium oxide nanocrystals as a function of nanocrystal diameter and surface coating. *ACS Nano* **2013**, *7*, 9693–9703. [[CrossRef](#)] [[PubMed](#)]
186. He, L.; Liang, B.L.; Li, L.; Yang, X.F.; Huang, Y.Q.; Wang, A.Q.; Wang, X.D.; Zhang, T. Cerium-oxide-modified nickel as a non-noble metal catalyst for selective decomposition of hydrous hydrazine to hydrogen. *ACS Catal.* **2015**, *5*, 1623–1628. [[CrossRef](#)]
187. Cargnello, M.; Doan-Nguyen, V.V.; Gordon, T.R.; Diaz, R.E.; Stach, E.A.; Gorte, R.J.; Fornasiero, P.; Murray, C.B. Control of metal nanocrystal size reveals metal-support interface role for ceria catalysts. *Science* **2013**, *341*, 771–773. [[CrossRef](#)]
188. Sun, C.W.; Li, H.; Chen, L.Q. Nanostructured ceria-based materials: Synthesis, properties, and applications. *Energy Environ. Sci.* **2012**, *5*, 8475–8505. [[CrossRef](#)]
189. Zhang, Z.; Lu, Z.H.; Tan, H.; Chen, X.; Yao, Q. CeO<sub>x</sub>-modified RhNi nanoparticles grown on rGO as highly efficient catalysts for complete hydrogen generation from hydrazine borane and hydrazine. *J. Mater. Chem. A* **2015**, *3*, 23520–23529. [[CrossRef](#)]
190. Li, Y.T.; Zhang, X.L.; Peng, Z.K.; Liu, P.; Zheng, X.-C. Highly efficient hydrolysis of ammonia borane using ultrafine bimetallic RuPd nanoalloys encapsulated in porous g-C<sub>3</sub>N<sub>4</sub>. *Fuel* **2020**, *277*, 118243. [[CrossRef](#)]
191. Chen, S.J.; Meng, L.; Chen, B.X.; Chen, W.Y.; Duan, X.Z.; Huang, X.; Zhang, B.S.; Fu, H.B.; Wan, Y. Poison tolerance to the selective hydrogenation of cinnamaldehyde in water over an ordered mesoporous carbonaceous composite supported Pd catalyst. *ACS Catal.* **2017**, *7*, 2074–2087. [[CrossRef](#)]
192. Li, X.Y.; Song, L.H.; Gao, D.W.; Kang, B.T.; Zhao, H.Q.; Li, C.C.; Hu, X.; Chen, G.Z. Tandem of Ammonia Borane Dehydrogenation and Phenylacetylene Hydrogenation Catalyzed by CeO<sub>2</sub> Nanotube/Pd@MIL-53 (Al). *Chem. A Eur. J.* **2020**, *26*, 4419–4424. [[CrossRef](#)]
193. Ruiz, A.M.; Sakai, G.; Cornet, A.; Shimano, K.; Morante, J.R.; Yamazoe, N. Microstructure control of thermally stable TiO<sub>2</sub> obtained by hydrothermal process for gas sensors. *Sens. Actuators B Chem.* **2004**, *103*, 312–317. [[CrossRef](#)]
194. Yousef, A.; Barakat, N.A.; Kim, H.Y. Electrospun Cu-doped titania nanofibers for photocatalytic hydrolysis of ammonia borane. *Appl. Catal. A Gen.* **2013**, *467*, 98–106. [[CrossRef](#)]
195. Carp, O.; Huisman, C.L.; Reller, A. Photoinduced reactivity of titanium dioxide. *Prog. Solid State Chem.* **2004**, *32*, 33–177. [[CrossRef](#)]
196. Rakap, M.; Kalu, E.E.; Özkar, S. Hydrogen generation from the hydrolysis of ammonia borane using cobalt-nickel-phosphorus (Co–Ni–P) catalyst supported on Pd-activated TiO<sub>2</sub> by electroless deposition. *Int. J. Hydrog. Energy* **2011**, *36*, 254–261. [[CrossRef](#)]
197. Shu, H.F.; Lu, L.L.; Zhu, S.F.; Liu, M.M.; Zhu, Y.; Ni, J.Q.; Ruan, Z.H.; Liu, Y. Ultra small cobalt nanoparticles supported on MCM41: One-pot synthesis and catalytic hydrogen production from alkaline borohydride. *Catal. Commun.* **2019**, *118*, 30–34. [[CrossRef](#)]
198. Lu, L.L.; Zhang, H.J.; Zhang, S.W.; Li, F.L. A family of high-efficiency hydrogen-generation catalysts based on ammonium species. *Angew. Chem. Int. Ed.* **2015**, *54*, 9328–9332. [[CrossRef](#)] [[PubMed](#)]
199. Zhang, Y.; Wang, M.S.; Zhu, E.B.; Zheng, Y.B.; Huang, Y.; Huang, X.Q. Seedless growth of palladium nanocrystals with tunable structures: From tetrahedra to nanosheets. *Nano Lett.* **2015**, *15*, 7519–7525. [[CrossRef](#)] [[PubMed](#)]
200. Chen, G.X.; Xu, C.F.; Huang, X.Q.; Ye, J.Y.; Gu, L.; Li, G.; Tang, Z.C.; Wu, B.H.; Yang, H.Y.; Zhao, Z.P.; et al. Interfacial electronic effects control the reaction selectivity of platinum catalysts. *Nat. Mater.* **2016**, *15*, 564–569. [[CrossRef](#)] [[PubMed](#)]
201. Huang, X.Q.; Tang, S.H.; Mu, X.L.; Dai, Y.; Chen, G.X.; Zhou, Z.Y.; Ruan, F.X.; Yang, Z.Y.; Zheng, N.F. Freestanding palladium nanosheets with plasmonic and catalytic properties. *Nat. Nanotechnol.* **2011**, *6*, 28. [[CrossRef](#)]

202. Zhang, H.; Jin, M.S.; Xia, Y.N. Noble-metal nanocrystals with concave surfaces: Synthesis and applications. *Angew. Chem. Int. Ed.* **2012**, *51*, 7656–7673. [[CrossRef](#)]
203. Song, J.; Gu, X.J.; Cheng, J.; Fan, N.; Zhang, H.; Su, H.Q. Remarkably boosting catalytic H<sub>2</sub> evolution from ammonia borane through the visible-light-driven synergistic electron effect of non-plasmonic noble-metal-free nanoparticles and photoactive metal-organic frameworks. *Appl. Catal. B Environ.* **2018**, *225*, 424–432. [[CrossRef](#)]
204. Huang, X.Q.; Tang, S.H.; Zhang, H.H.; Zhou, Z.Y.; Zheng, N.F. Controlled formation of concave tetrahedral/trigonal bipyramidal palladium nanocrystals. *J. Am. Chem. Soc.* **2009**, *131*, 13916–13917. [[CrossRef](#)] [[PubMed](#)]
205. Xie, S.F.; Zhang, H.; Lu, N.; Jin, M.S.; Wang, J.G.; Kim, M.J.; Xie, Z.X.; Xia, Y.N. Synthesis of rhodium concave tetrahedrons by collectively manipulating the reduction kinetics, facet-selective capping, and surface diffusion. *Nano Lett.* **2013**, *13*, 6262–6268. [[CrossRef](#)] [[PubMed](#)]



© 2020 by the authors. Licensee MDPI, Basel, Switzerland. This article is an open access article distributed under the terms and conditions of the Creative Commons Attribution (CC BY) license (<http://creativecommons.org/licenses/by/4.0/>).